5-2024

Quantifying the Role of Karst Groundwater on Mountain River Discharge

Devon Hill
Utah State University, devin.hill@usu.edu

QUANTIFYING THE ROLE OF KARST GROUNDWATER ON MOUNTAIN RIVER DISCHARGE

by

Devon Hill

A thesis submitted in partial fulfillment of
the requirements for the degree

of

MASTER OF SCIENCE

in

Civil and Environmental Engineering

Approved:

Bethany T. Neilson, Ph.D. Major Professor	Tianfang Xu, Ph.D. Committee Member
Dennis L. Newell, Ph.D. Committee Member	D. Richard Cutler, Ph.D. Vice Provost of Graduate Studies

UTAH STATE UNIVERSITY
Logan, Utah

2024

ABSTRACT

Quantifying the Role of Karst Groundwater on Mountain River Discharge

by

Devon Hill, Master of Science

Utah State University, 2024

Major Professor: Dr. Bethany T. Neilson
Department: Civil and Environmental Engineering

The effects of climate change on heterogeneous karst systems are primarily studied and projected via large karst spring dynamics. These studies often omit other basin-wide surface-groundwater exchanges, in particular distributed groundwater inflows to streams and losses back to the aquifer. These exchanges are significant and represent an important element of karst aquifer recharge and discharge. High spatial resolution sampling of the Logan River enabled reach-scale mass balances to isolate these groundwater exchanges. Distributed groundwater inflow solute concentrations, calculated by solute mass or isotope ratio balances, provided input to an equilibrium model which estimated saturation indices of prevalent minerals in the distributed groundwater inflows. Multiple principal component analyses, utilizing various subsets of data, were used to compare distributed groundwater inflows to other flow sources and helped partition springs as karst conduit or matrix dominated flow paths. The partitioning of springs informed more intensive mass balances which quantified the karst conduit and matrix components of distributed groundwater inflows. Two synoptic samplings, one under

snowmelt conditions and one at baseflow conditions, captured a glimpse of watershed seasonal variation. Distributed groundwater inflows were found to be temporally and spatially variable, but most of the variation was expected due to karst aquifer heterogeneity and the seasonal dynamics of the snow-dominated watershed. Saturation indices and principal component analyses of river, spring, and distributed groundwater inflows suggest distributed groundwater inflows are most similar to springs, in particular the karst conduit dominated springs. Distributed groundwater inflows were also predominantly karst with an increased matrix component during baseflow conditions. These findings suggest the magnitude of distributed groundwater inflows is a significant fraction of river discharge that cannot be ignored; however, spring chemistry may be extrapolated to distributed groundwater inflows. Because karst conduit flow paths typically have short residence times, they are susceptible to climate change and pollution. The findings of this work suggest that a large fraction of river flow in karst systems can be derived from distributed groundwater inflow that is similarly vulnerable to these influences.

(77 pages)

PUBLIC ABSTRACT

Quantifying the Role of Karst Groundwater

on Mountain River Discharge

Devon Hill

A primary objective of hydrological research is to anticipate the shifts in water supply due to climate change. These shifts are difficult to predict in karst areas like Logan Canyon because much of the water moves through large fractures and cave networks that transport groundwater quickly, but there are some groundwater fractions which move very slowly. Many studies in karst regions use spring dynamics to assess aquifer condition, but overlook other influences such as exchanges between a river and the underlying aquifer. In this study, we calculated the quantity and chemical makeup of these groundwater and surface water exchanges by measuring the flow and chemistry of all surface inputs (tributaries and springs) and losses (diversions) from the river. Based on this sampling and calculations that track all the ins and outs that occur over small river segments, groundwater exchanges were found to vary significantly throughout the river system. In some cases, groundwater inflows occurred in one segment and adjacent segments showed significant losses to the aquifer. Using the calculated chemistry of groundwater inflows to the river, we determined they are mostly comparable to springs sourced from fast-transporting karst networks. These findings suggest water supply in karst regions may be less resilient to extended periods of drought and multiple years of low snowpack relative to other groundwater aquifers because river discharge is mainly sourced from fracture and cave networks which drain quickly.

ACKNOWLEDGMENTS

I would like to thank the students, faculty, and staff at the UWRL who have helped me feel part of a meaningful organization. I would like to thank the UWRL EQL, Joan McLean, Marissa Li, the USU Geosciences Stable Isotope Lab, Audrey Warren, the BSU Isotope Geology Lab, and Nathaniel Ashmead for the heaps of lab analysis they have done. Many individuals assisted in data collection: Dr. Pin Shuai, Jihad Othman, Michael Laswell, Patrick Strong, Abbygael Johnson, Abby Englund, Chelsey Cowburn, Dr. Bethany Neilson, Hyrum Tennant, Dr. Dennis Newell, Seohye Choi, Dr. Tianfang Xu, Nathaniel Ashmead, and Dr. James McNamara.

My committee members, Dr. Dennis Newell and Dr. Tianfang Xu, provided useful and kind guidance throughout my research. I would like to thank them for their optimism and genuine interest in my work. Dr. Bethany Neilson is an excellent mentor, a constant source of encouragement, and truly kind. She was relentless in striving to understand our research and me. I would like to thank her for all she has done for me and taught me.

Patrick Strong, Abbygael Johnson, Abby Englund, Chelsey Cowburn, and Hyrum Tennant taught me how to do hydrological field work and welcomed me into the Neilson Lab. Hyrum Tennant and Michael Laswell have been examples to me and set a high standard, I would like to thank them for the conversations and support. Carson Goodrich and Ty Koppenhafer have been great friends and important influences on my studies. Lastly, I'd like to thank my wife, parents, and siblings for sustaining me through school. Each of them played a critical role in shaping who I am.

This research was supported with funding from the National Science Foundation grant numbers 2014336, 2044051, and 2043150.

CONTENTS

LIST OF FIGURES

Page

LIST OF TABLES

Page

1 INTRODUCTION

Climate change is altering hydrologic responses worldwide with impacts ranging from prolonged drought (Dai, 2011), to extreme precipitation events (Gimeno et al., 2022), to changing snow accumulation (Barnett et al., 2005; Knowles et al., 2006; Mote et al., 2005). Karst hydrology, dominated by interconnected solution-enhanced groundwater pathways in carbonate rock, is prevalent around the world (Goldscheider et al., 2020) with approximately 9% of the global population consuming water from karst aquifers (Stevanović, 2019). Given the prevalence of and dependence on karst aquifers, anticipating the effects of climate change on these systems is critical. However, climate change can affect karst aquifers differently because they develop in diverse regions (Veress, 2020), ranging from lush tropical (Klaas et al., 2020) to harsh alpine climates (Smart, 2003). Alpine and mountainous karst hydrologic responses have historically been dominated by snow accumulation and melt processes (Gremaud & Goldscheider, 2010; Hottelet et al., 1993; Jódar et al., 2020), but climate change induced shifts from snowmelt to rain dominated precipitation will alter hydrologic responses and water availability (Klos et al., 2014; Knowles et al., 2006; López-Moreno et al., 2021; Tennant et al., 2015).

Uncertainty of climate change effects on these and other karst systems is largely due to their heterogeneity (Hartmann et al., 2017). Karst systems, even in similar regional or climatic conditions, develop uniquely based on structural geology (i.e., fractures, folds, dips) (Goldscheider, 2005), stratigraphy (Brezinski, 2007), and rock types (Veress, 2020). Additionally, each karst aquifer has high intra-system heterogeneity (Bakalowicz, 2005). Karst aquifers may store a mixture of water with subannual (Land & Timmons, 2016; Spangler, 2001; Spellman et al., 2022) to millennial residence times (Bethke & Johnson,

2008; Musgrove et al., 2019). The disparate residence times are due to a range of porosities from bulk rock porosity (primary) to solution-enhanced fractures or conduits (tertiary porosity) (Ford & Williams, 2007; Land & Timmons, 2016). Here we will refer to flow through tertiary porosity as “karst” flow and assign the umbrella term “matrix” flow to flow through primary porosity, secondary porosity (fractures), and porous media (Neilson et al., 2018). Unique system development and the disparate residence times between karst flow and matrix flow make it difficult to understand karst aquifer connectivity and controls, making the anticipation of climate change impacts on hydrologic responses even more challenging.

Current projections for karst watershed response to climate change and general understanding of the temporal patterns in karst aquifers is mainly derived from studies on karst springs (Donovan et al., 2022; Fiorillo, 2014; Fiorillo et al., 2021; Nerantzaki & Nikolaidis, 2020). While springs are a primary source of karst groundwater discharge, these studies omit any other basin-wide connectivity between groundwater and surface water. This sort of spring centric understanding is due in part to the relative ease of monitoring springs and the dependence on springs for water supply (Baudement et al., 2017; Bonacci et al., 2018; Spangler, 2001). Spring studies have primarily been motivated by the intent to protect water supply by identifying recharge areas and delineating groundwater basins that supply the springs (Civita, 2008; Farics et al., 2021). Many prior studies have established connections between multiple springs sourced from the same aquifer (e.g., Lastennet & Mudry, 1997; Minvielle et al., 2015), however there is limited work focused on obtaining a holistic view of the connections between karst

groundwater and surface water. In particular, relatively few studies in karst regions directly investigate the distributed groundwater exchanges.

Both distributed groundwater inflows (DGI) and distributed groundwater losses (DGL) have been shown to be significant in some karst watersheds (Bailly-Comte et al., 2009; Glaser et al., 2020; Groten & Alexander, 2015; Keshavarzi et al., 2017; Khadka et al., 2017; Neilson et al., 2018). For example, Neilson et al. (2018) and Groten & Alexander (2015) showed significant contributions to streamflow from sources other than measured springs and tributaries. Both used mass balances and incremental flow gaging (a simple type of mass balance) to estimate DGI and DGL, though there are other methods for estimating exchanges. These include point measurements, Darcy flow approximations, and energy balances (Kalbus et al., 2006). However, point measurements of DGI are not broadly applicable in karst because it is heterogeneous and point measurements cannot be accurately extrapolated to the rest of the stream (Bakalowicz, 2005; Khadka et al., 2017). Karst aquifer heterogeneity further creates disparate hydraulic conductivities between layers as well as open channel or pressurized flow through karst conduits (Kaufmann et al., 2014; Perne et al., 2014; Zoghbi & Basha, 2019), resulting in discontinuous head throughout the aquifer and violating Darcy flow approaches. Energy balances are not nullified by karst properties and can provide information about the quantity of DGI and DGL. However, combining flow and solute or isotope mass balances result in information about the chemical signature of DGI and subsurface hydrologic connectivity. The chemical signature estimated by these mass balances can then be interpreted to identify the contributions of karst and matrix flow to DGI (Neilson et al., 2018) and provide greater insight regarding flow paths and residence time.

Since karst and matrix flow components of DGI will likely respond differently to climate change and DGI has been shown to be a substantial contributor to streamflow, the need for better understanding and constraining karst and matrix flow components of DGI is clear. Additionally, initial effects of climate change will likely be subtle given the high seasonal variation in karst aquifer contributions to surface water (Pulido-Bosch et al., 1995; Wang et al., 2020). This highlights the need to establish a baseline of DGI seasonal variation, particularly in snowmelt driven, mountainous karst watersheds. To address these needs, this paper investigates the components and variability of DGI via flow, ion, and isotope mass balances using synoptic data collected at high spatial resolution during high flow recession and baseflow conditions in a highly karstified mountainous watershed in northern Utah. Our objectives are to study the spatial and seasonal variability in DGI, understand the relationship between DGI springs and river water, and quantify the matrix and karst components of DGI to better understand aquifer resiliency.

2 STUDY AREA

The Logan Canyon watershed in northern Utah and southern Idaho (Fig. 1) is a 554 km^2 catchment that is made up of approximately 71% carbonate rock (limestone and dolostone) with typical karst features (e.g., springs, sinkholes, caves). The watershed is mountainous with elevation ranging from 1422 m to 3041 m. More precipitation falls at higher elevations (125 cm) than low (45 cm), and the majority currently falls as snow (Neilson et al., 2021).

The main watercourse is the third order Logan River, with an average gradient of 1.7%, though river grade and sinuosity vary throughout the canyon. The headwater location shifts between the M56.95 (elevation of 2460 m) in the spring to S44.48 km (elevation of 2185 m) during the late summer due to less groundwater inflow (Fig. 1). River flow is augmented by dozens of springs and three major tributaries (T14.79, T26.03, T39.18) throughout the watershed (Fig. 1). The river flows freely until R1 where there are three small dams (Fig. 1). Amid these dams, water is rerouted through a hydroelectric power plant before returning to the river. Additionally, there is a large agricultural diversion (Highline Canal, D2.07, USGS 10108400) before the long term USGS station at the mouth of the canyon (300 m upstream of M0.0, USGS 10109000). Including the water diverted, the annual average river discharge is 6.9 m^3s^{-1} (referred to as cms throughout) with large seasonal variation between high flows during the spring snowmelt (annual peaks averaging above 26 cms) and baseflows from August-March (averaging 2.2 cms).

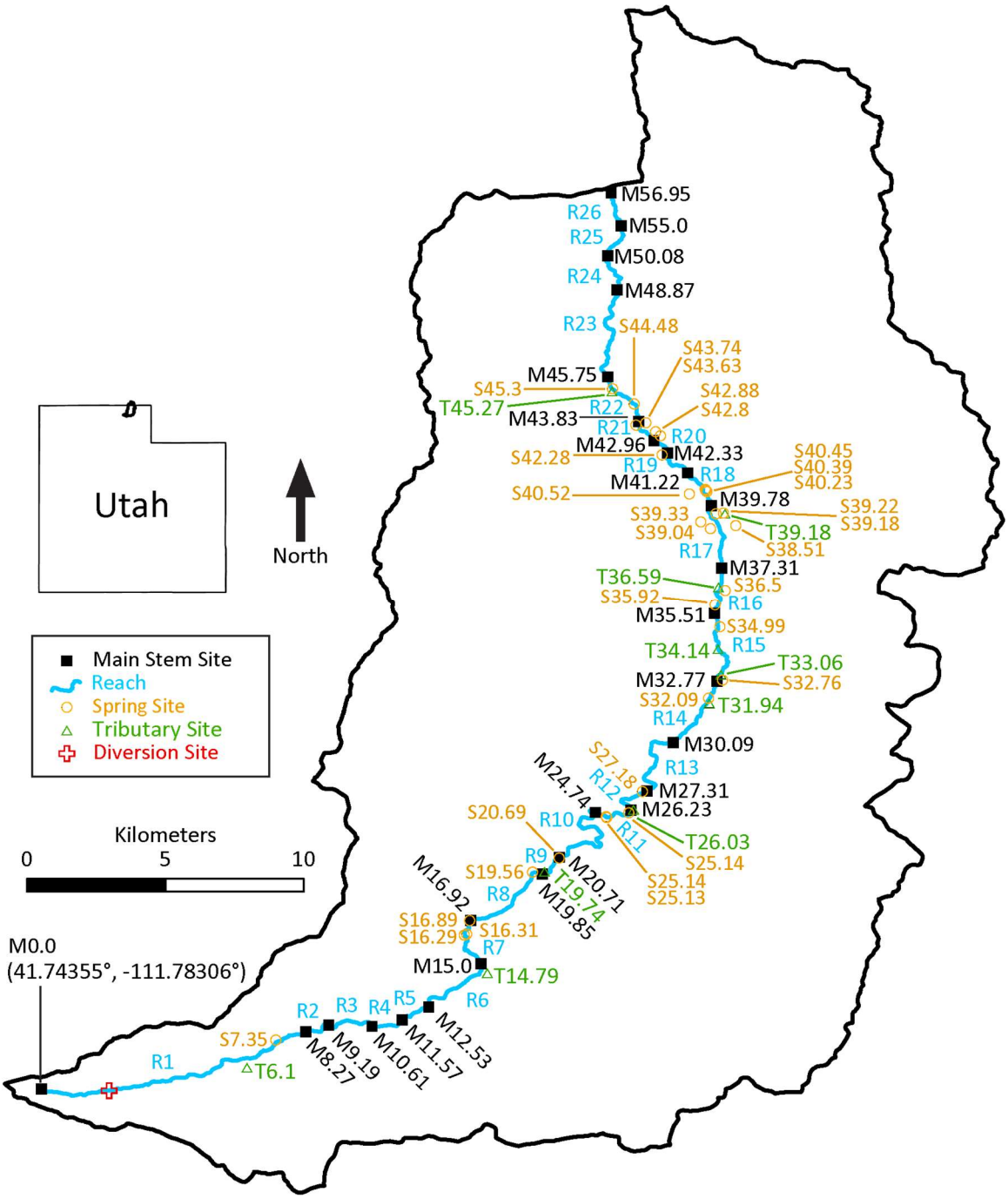

Fig. 1. Watershed boundary with the reaches numbered starting at the mouth of the canyon. The main stem sites are denoted with an “M” followed by their distance upriver from the most downstream site M0.0. The springs, “S”; tributaries, “T”; and diversion “D” follow the same convention. A table relating these codes to local names is available in the appendix (Table B 1).

A sizable portion of snowmelt reaches the river via DGI (Neilson et al., 2018) and springs which are controlled hydrologically largely by geologic stratigraphy and structures (e.g., Bahr, 2016). The stratigraphy is primarily Paleozoic Era limestone and dolostone with minor siliciclastic intervals, with a Tertiary Period disconformity and conglomerate on top in many areas (Dover, 1995). The variably karstified carbonate formations contain aquifers separated by the siliciclastic formations. The Logan Peak syncline funnels groundwater along its southward plunge until the aquifer-containing units surface, producing large springs along Logan River. Tracer studies have demonstrated travel times, from sinkholes or losing streams to springs, ranging from 8 to 31 days (Spangler, 2001).

3 METHODS

DGI and DGL have been shown to be substantial components of the Logan River flow regime (Neilson et al. 2018), though they cannot be measured directly, and they vary over space and time. A combination of flow and mass balances provide insight regarding DGI that can be useful for understanding flow paths, sources, and inferring residence times (Neilson et al., 2018; Tennant et al., 2021).

3.1 Mass Balances

3.1.1 Flow Balance

The simplest mass balance, incremental streamflow or flow balance method, accounts for all measurable exchanges with a reach such as springs, tributaries, and diversions; and assumes the remaining exchange is due to the net difference in DGI and DGL (Eqn. 1).

$$Q_{NET} = Q_{US} + Q_{TRIB} - Q_{DS} - Q_{DIV} \quad \text{Eqn. 1}$$

The flow balance (Fig. 2A, Eqn. 1) estimates the net change in discharge in the stream reach (Q_{NET}) by differencing the discharge at the upstream site of the reach (Q_{US}) and the downstream site of the reach (Q_{DS}) while accounting for measurable inflows (Q_{TRIB}) and measurable outflows (Q_{DIV}). Eqn. 1 assumes the reach and all components are in steady state. Additionally, assuming all unmeasured inflows and outflows are between the groundwater and the river means:

$$Q_{NET} = Q_{DGI} - Q_{DGL} \quad \text{Eqn. 2}$$

Where Q_{DGI} is the DGI discharge and Q_{DGL} is the DGL discharge.

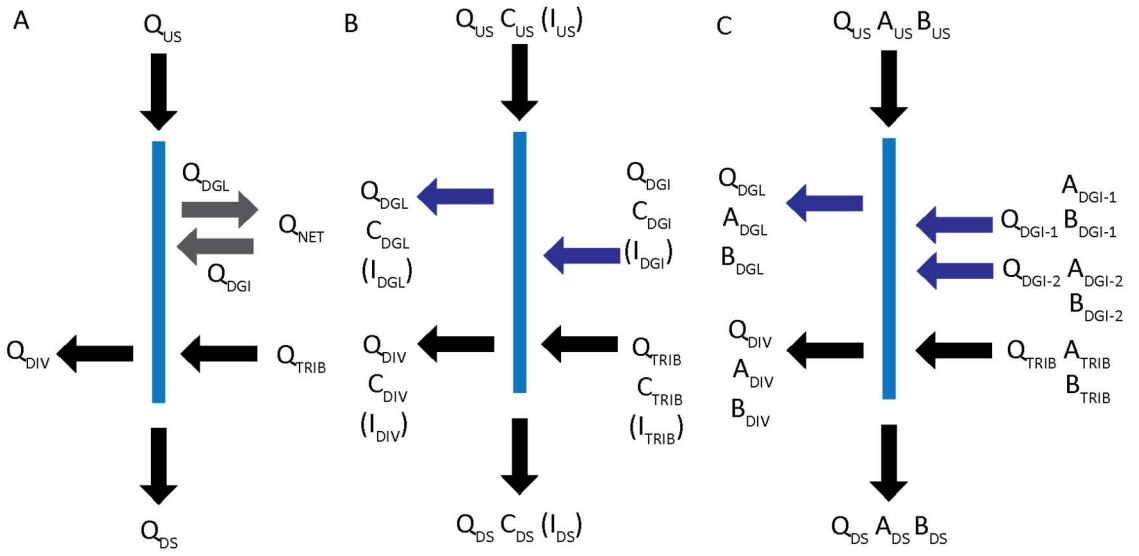

Fig. 2. Line diagram of a stream reach showing components of a flow balance (A). Q_{US} is the measured discharge at the upstream side of the reach. Q_{DS} is the measured discharge at the downstream side of the reach. Q_{TRIB} represents the total of all measured inflows (i.e., tributaries and springs). Q_{DIV} represents the total of all measured outflows via diversions from the reach. Q_{NET} is the difference in discharge between the Q_{DGI} and Q_{DGL} (Eqn. 2). The reach line diagram when accounting for Q_{DGI} and Q_{DGL} individually, representing the one-solute balance with solute C and representing the one-isotope balance with solute C and solute isotope I (B). The reach line diagram accounting for two distinct DGIs (Q_{DGI-1}, Q_{DGI-2}), representing the two-solute balance with solute A and solute B (C).

3.1.2 One-Solute Balance

A solute mass balance can be combined with a flow balance, here referred to as a one-solute balance, to calculate gross Q_{DGI} and Q_{DGL}. Accounting for both Q_{DGI} and Q_{DGL} individually (Fig. 2B), the flow balance (Eqn. 1) becomes:

$$Q_{US} + Q_{TRIB} + Q_{DGI} = Q_{DS} + Q_{DIV} + Q_{DGL} \quad \text{Eqn. 3}$$

Eqn. 3 requires the same assumptions as Eqn. 1 (steady state) and Eqn. 2 (all unmeasured loss is Q_{DGL} and all unmeasured gain is Q_{DGI}). Since neither of the gross groundwater exchanges (Q_{DGI}, Q_{DGL}) are known, an additional equation, a solute mass

balance (Eqn. 4), can be evaluated in a system of equations (Eqn. 3, Eqn. 4) to establish gross groundwater exchanges.

$$Q_{US}C_{US} + Q_{TRIB}C_{TRIB} + Q_{DGI}C_{DGI} = Q_{DS}C_{DS} + Q_{DIV}C_{DIV} + Q_{DGL}C_{DGL} \qquad \text{Eqn. 4}$$

Where C is the concentration of a solute (e.g., if the solute were chloride, C_{US} would be the concentration of chloride in the stream at the upstream site). Eqn. 4 assumes the reach and all components are in steady state (discharge and solute concentration), mixed conditions exist at all sample sites, the solute is conservative throughout the reach during sampling, all unmeasured inflow is homogeneous groundwater, and all unmeasured loss is homogeneous.

An additional assumption makes the system of equations more manageable by assigning a value to the DGL solute concentration (C_{DGL}). Following Payn et al. (2009), one can assume all the inflows to the reach (Q_{US}, Q_{TRIB}, Q_{DGI}) occur before Q_{DGL} (IO), then the C_{DGL} would be the same as the C_{DS}. Conversely, if DGL occurs before the inflows (OI) (Fig. 2B), then the C_{DGL} would be the same as the C_{US}. Either one of these assumptions, in-before-out (IO) or out-before-in (OI), leaves three remaining unknowns in the system of equations (Eqn. 3, Eqn. 4): Q_{DGI}, C_{DGI}, and Q_{DGL}.

The DGI and DGL discharges (Q_{DGI}, Q_{DGL}) can be estimated by iterating through possible DGI solute concentrations (C_{DGI}). If the associated Q_{DGI} and Q_{DGL} are positive and Q_{DGL} is no greater than an assumed maximum value, then the solution is viable. After iterating through all reasonable C_{DGI}, the result of the mass balance is three distributions of solutions for the three unknowns (Q_{DGI}, C_{DGI}, Q_{DGL}).

3.1.3 One-Isotope Balance

While this approach works for solute concentrations, additional information on groundwater behavior can be contained in isotope ratios. Therefore, an isotope balance (Eqn. 5), adapted from Faure (1986), can be applied with the one-solute balance (Eqn. 3, Eqn. 4) results (Q_{DGI}, C_{DGI}, Q_{DGL}) to estimate the isotope ratio of a solute in DGI. Here, this system of equations is referred to as a one-isotope balance.

$$Q_{US}C_{US}I_{US} + Q_{TRIB}C_{TRIB}I_{TRIB} + Q_{DGI}C_{DGI}I_{DGI} = Q_{DS}C_{DS}I_{DS} + Q_{DIV}C_{DIV}I_{DIV} + Q_{DGL}C_{DGL}I_{DGL} \quad \text{Eqn. 5}$$

Where I is the ratio of two isotopes of the solute with concentration C. Eqn. 5 requires the same assumptions as the flow (Eqn. 3) and solute mass balance (Eqn. 4). Additionally, Eqn. 5 assumes steady solute isotope conditions, mixed solute isotope conditions exist at sample sites, solute isotope composition is conservative throughout the reach during sampling, DGI solute isotope composition is homogeneous, and DGL solute isotope composition is homogeneous.

Two additional approximations are necessary in Eqn. 5. First, the weighted average atomic mass of solute isotopes in each component (Q_{US}, Q_{TRIB}, Q_{DGI}, Q_{DGL}, Q_{DIV}, Q_{DS}) is equal (Faure, 1986). Second, the abundance of the denominator isotope (e.g., ^{86}Sr in ^{87}Sr/^{86}Sr or ^{238}U in ^{234}U/^{238}U) is equal in each component (Faure, 1986). After these additional approximations, the IO or OI assumption is applied to assign a reasonable solute isotope composition to the DGL (I_{DGL}). Finally, the only unknown remaining is the DGI solute isotope ratio (I_{DGI}).

The isotope balance (Eqn. 5) filters the results of the one-solute balance (Q_{DGI}, C_{DGI}, Q_{DGL}) by ensuring the associated I_{DGI} is within a reasonable range. The result of the

isotope balance is distributions of solutions for the four unknowns (Q_{DGI}, C_{DGI}, I_{DGI}, Q_{DGL}).

3.1.4 Two-Solute Balance

The one-solute and one-isotope balances assume all DGI comes from the same groundwater source; however, to identify contributions from two separate groundwater sources a two-solute balance can be used (Tennant et al., 2021). A two-solute balance comprises three equations: flow balance (Eqn. 6), and two different solute mass balances (Eqn. 7, Eqn. 8).

$$Q_{US} + Q_{TRIB} + Q_{DGI-1} + Q_{DGI-2} = Q_{DS} + Q_{DIV} + Q_{DGL} \quad \text{Eqn. 6}$$

$$Q_{US}A_{US} + Q_{TRIB}A_{TRIB} + Q_{DGI-1}A_{DGI-1} + Q_{DGI-2}A_{DGI-2} = Q_{DS}A_{DS} + Q_{DIV}A_{DIV} + Q_{DGL}A_{DGL} \quad \text{Eqn. 7}$$

$$Q_{US}B_{US} + Q_{TRIB}B_{TRIB} + Q_{DGI-1}B_{DGI-1} + Q_{DGI-2}B_{DGI-2} = Q_{DS}B_{DS} + Q_{DIV}B_{DIV} + Q_{DGL}B_{DGL} \quad \text{Eqn. 8}$$

Where A and B are the concentrations of two different solutes and $DGI\text{-}1$ and $DGI\text{-}2$ are two DGI components (Fig. 2C). Like the one-solute balance, these equations assume steady flow and solute conditions, mixed conditions exist at all sample sites, the solutes are conservative throughout the reach during sampling, and all unmeasured loss is homogeneous and through the ground. Also, the IO or OI assumption is used to assign solute concentrations to both DGL solute concentrations (A_{DGL}, B_{DGL}), leaving seven remaining unknowns: both DGI discharges (Q_{DGI} , Q_{DGI-2}), both DGI solute concentrations for both solutes (A_{DGI-1}, A_{DGI-2}, B_{DGI-1}, B_{DGI-2}) and DGL discharge (Q_{DGL}).

The groundwater exchanges (Q_{DGI-1}, Q_{DGI-2}, Q_{DGL}) are estimated by iterating through possible combinations of DGI solute concentrations (A_{DGI-1}, A_{DGI-2}, B_{DGI-1}, B_{DGI-}). The possible DGI-1 and DGI-2 solute concentrations are incrementally sampled assuming a uniform distribution from an assumed range in their respective concentrations of solute A and solute B. If the associated groundwater exchange values are positive and the DGL discharge (Q_{DGL}) is no greater than an assumed value, then the solution is viable. After iterating through every combination of reasonable DGI solute concentrations (A_{DGI-1}, A_{DGI-2}, B_{DGI-1}, B_{DGI})., the result of the two-solute balance is seven distributions of solutions including two distributions of different DGI discharges (Q_{DGI-1}, Q_{DGI-2}), both DGI solute concentrations for both solutes (A_{DGI-1}, B_{DGI-1}, A_{DGI-2}, B_{DGI-2}), and DGL discharge (Q_{DGL}).

3.2 Synoptic Sampling

Attaining accurate estimates of quantity and chemistry of DGI with mass balances requires intensive data collection. Since DGI cannot be directly measured, all other components of the mass balances must be directly measured to quantify DGI. High resolution (reach-scale) flow and concentration sampling enables better understanding of spatial variation throughout the watershed while supporting DGI estimates and providing a clearer picture of basin scale water and mass balances.

Using the Logan River as a case study, two synoptic sampling campaigns were conducted in June and October 2022 (Fig. 3, Fig. 4). Necessary data were collected to evaluate flow, mass, and isotope balances at a reach scale to get at two high-resolution

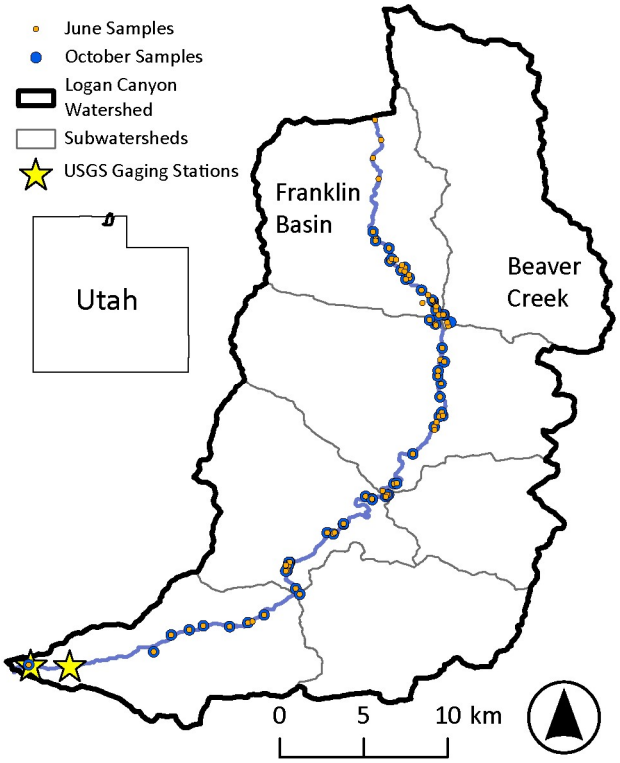

Fig. 3. Watershed boundaries for Logan River within Logan Canyon with the synoptic sampling locations for June 2022 (orange) and October 2022 (blue) labelled. The downstream star is USGS gaging station 10109000 on the Logan River. The upstream star is the USGS gaging station on the Highline Canal (10108400). The Franklin Basin and Beaver Creek subbasins are labelled because they are referenced throughout this document.

spatial snapshots of DGI. Together, both multi-day synoptic samplings provide a glimpse into the seasonal variation in streams, springs, and DGI. The mean discharge reported by the USGS (gage 10109000 plus gage 10108400) at the canyon mouth during the June event was 10.6 cms with a minimum flow of 9.22 cms and a maximum flow of 11.9 cms. The mean discharge during the October event was 2.4 cms with a minimum flow of 1.7 cms and a maximum flow of 2.7 cms.

Sampling locations in Logan River were selected primarily to segment the river into similarly sized reaches. Sampling locations were also selected to ensure mixed

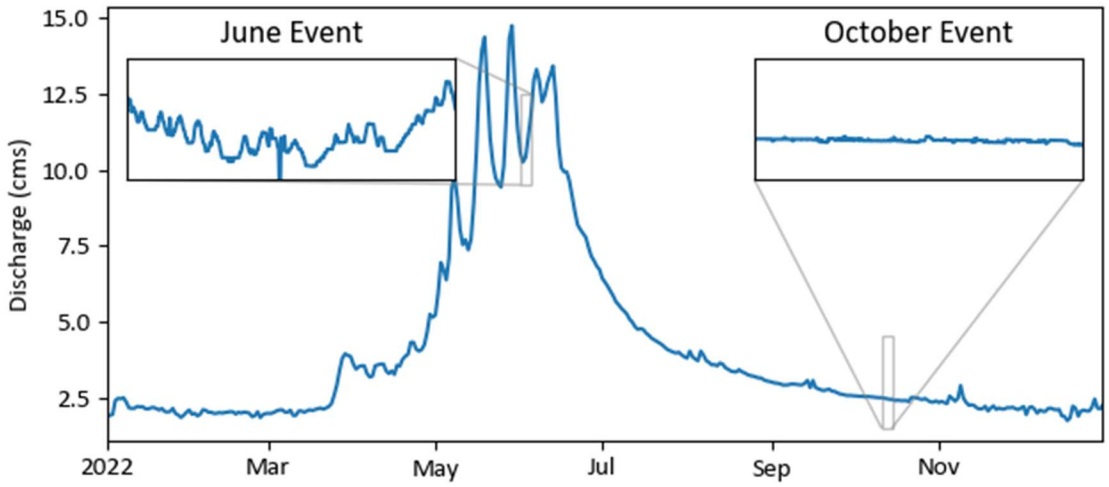

Fig. 4. Logan River discharge, USGS station 10109000 and 10108400 (Fig. 3) combined. Each subplot has different axis limits but are scaled equally in the x (time) and y (discharge) direction for ease of comparison.

conditions in the river. All known and measurable tributaries, spring inflows, and diversions to and from the mainstem reaches were measured to isolate and more precisely quantify DGI and DGL.

At every mainstem, tributary, spring, and diversion site, discharge and field water quality parameters (temperature, specific conductivity, pH, and dissolved oxygen) were measured, and chemistry grab samples were collected (Table B 2). Except for the USGS gaging locations (Fig. 3), river flow measurements were made using velocity-area measurements with a YSI SonTek FlowTracker2 Acoustic Doppler Velocimeter (ADV). Several minor tributary and spring discharges were measured using Hach FH950 Handheld Flow Meters due to shallow water limitations. A few very small spring discharges were visually estimated. One large spring (S16.89) discharge was estimated via differential gaging due to its highly distributed outlets.

In situ water quality parameters (temperature, specific conductivity, pH, and dissolved oxygen) were measured using a YSI 6920 V2 Sonde that was calibrated multiple times during each synoptic sampling event. Grab samples for Alkalinity, as $CaCO_3$, were collected in 125mL acid-washed high-density polyethylene (HDPE) bottles without headspace and analyzed at the lab using titration. Water samples for ion analysis were filtered with a 0.45-µm nylon filter into 60mL acid-washed HDPE bottles without headspace. Cation samples were acidified with concentrated trace-metal grade nitric acid (HNO_3) after transport to the lab. Cations (Na^+, Ca^{2+}, K^+, Mg^{2+}) were analyzed using inductively coupled plasma mass spectrometry (ICP-MS). Anions (Cl^-, NO_3^{2-}, PO_4^-, SO_4^{2-}) were analyzed using ion chromatography (IC). Water samples for strontium (Sr) and uranium (U) concentrations and isotope ratios ($^{87}Sr/^{86}Sr$, $^{234}U/^{238}U$) were filtered with a 0.2-µm nylon filter into 45mL acid-washed HDPE vials. These were acidified with nitric acid (HNO_3) after transport to the lab for preservation. Sr and U concentrations were analyzed using ICP-MS and the isotope ratios were analyzed using thermal ionization mass spectrometry (TIMS). All samples were immediately placed in coolers until transported to the lab where they were frozen or refrigerated until analysis.

Though flow conditions in June were unstable relative to the flow in October (Fig. 4), every effort was made to ensure steady conditions while measurements were taken for each reach. One team sequentially measured discharge on the mainstem of the river, requiring approximately one hour per measurement. Simultaneously, two other teams measured discharge of inflows to the reach and two water quality teams took samples of mainstem and inflows. At the beginning of each sampling day a duplicate discharge measurement for the last mainstem site from the preceding day was taken to ensure stable

and representative flow conditions for every reach's flow balance. Finally, sampling protocols were established to ensure the fully mixed assumption was met. All water quality and grab sample measurements were taken from well mixed parts of the river. Spring samples were taken from the heads of springs or as close as possible.

To establish the sources and contributions of DGI, a series of steps were completed to first calculate the DGI throughout the watershed and then relate it to other data collected (Fig. 5).

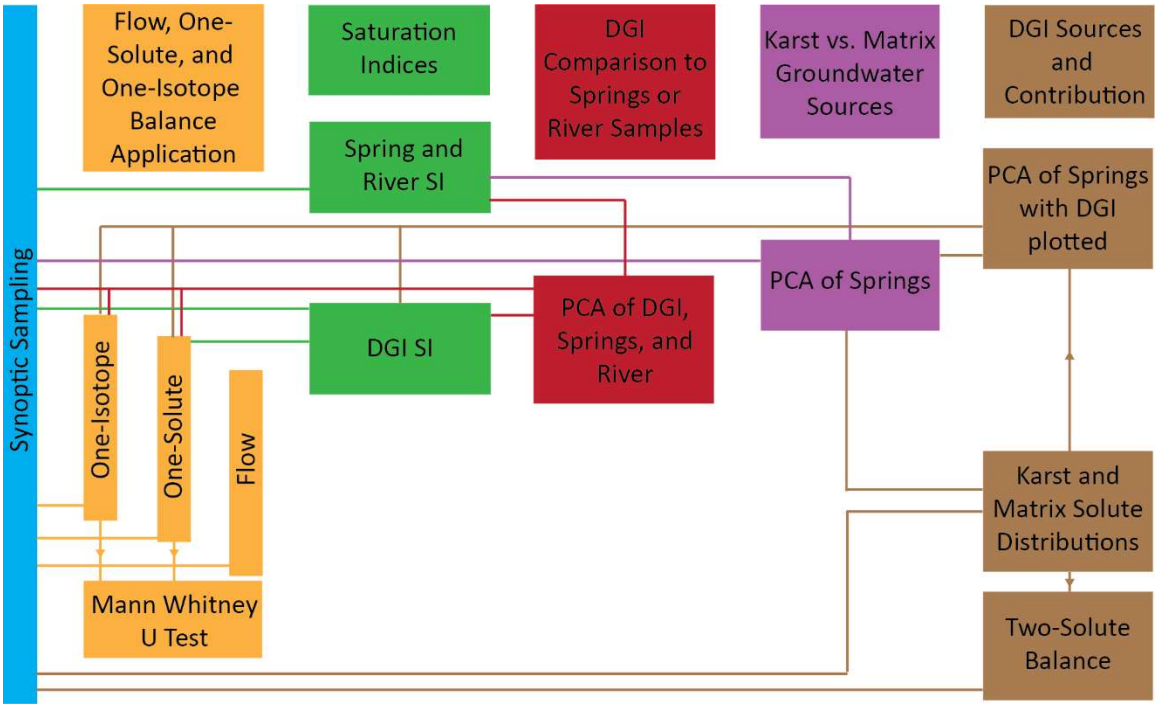

Fig. 5. Methodology flow chart.

3.3 Flow, One-Solute, and One-Isotope Balance Application

After completing the synoptic sampling events, flow, one-solute, and one-isotope balances were used to calculate the Q_{NET}, Q_{DGI}, Q_{DGL}, and DGI chemical characteristics (C_{DGI}, I_{DGI}) in every reach for both events. First, the flow balance was used to calculate

the net groundwater exchanges to provide a baseline for the gross groundwater exchanges. Then, for every reach, estimates from nine one-solute balances using Na^{+}, Ca^{2+}, K^{+}, Mg^{2+}, Cl^{-}, SO_4^{2-}, Alkalinity as $CaCO_3$, Sr, and U, respectively, were compared. Considering both sample periods, the largest net groundwater loss (1 cms) provided a cap on the acceptable Q_{DGL} values. C_{DGI} ranges were established from the minimum and maximum observed concentration throughout the watershed. Sampling from an assumed uniform C_{DGI} distribution, 100,000 one-solute balances were completed for each reach in both sample periods. Results using the OI assumptions were evaluated.

The one-isotope balances using $^{87}Sr/^{86}Sr$ and $^{234}U/^{238}U$ follow the same procedure and assumptions as the one-solute balances. Following, the calculations to estimate I_{DGI}, the results were filtered to only report solutions with I_{DGI} within the range of solute isotope ratios measured throughout the watershed during each sampling period.

Following the completion of one-isotope and one-solute balances, the resulting distributions from June were compared to October to see if there was seasonal variation. For example, the Q_{DGI} distribution calculated by the one-solute balance of R1 in June was compared to the Q_{DGI} distribution calculated by the one-solute balance of R1 in October. The nonparametric Mann Whitney U test was used to assess if there was statistically significant difference between the two distributions (Mann & Whitney, 1947). Due to the number of iterations required for the Mann Whitney U test, the one-solute and one-isotope balances were recomputed with only 200 iterations rather than 100,000. The null hypothesis that the October DGI value (Q_{DGI}, Q_{DGL}, C_{DGI}, or I_{DGI}) was from the same population as the June DGI value was rejected if either of the alternatives (October > June or October < June) had an associated p-value greater than 0.99.

3.4 Saturation Indices

The distributions of C_{DGI} and I_{DGI} are useful for understanding the range of solute concentrations and isotope ratios possible in Q_{DGI}. These ranges can be used to identify end members if solute concentrations or isotope ratios are distinct (Doctor et al., 2006; Long & Valder, 2011). However, groundwater solute concentrations are not just a function of the media through which it traveled but also a function of actual concentrations relative to saturation values for relevant minerals (Drever, 1988). Mineral saturation of carbonate minerals (e.g., calcite, dolomite) is strongly influenced by the speciation of dissolved carbonate ions and pH (Drever, 1988; Minvielle et al., 2015).

To obtain a more holistic view of the water-rock interactions affecting groundwater solute concentrations, an approximate saturation index (SI) of prevalent minerals in the watershed (dolomite (SI_D) and calcite (SI_C)) and the partial pressure of CO_2 (P_{CO2}) were calculated for DGI, springs, and river water. Using water quality and chemistry grab sample results, the saturation indices for springs and river water were established using PHREEQC (Parkhurst & Appelo, 2013). However, while the concentrations of key DGI solutes were estimated in the one-solute balances, an additional step was necessary to compile the distributions of C_{DGI} for each reach prior to using PHREEQC. This was completed via a simple mapping of solute concentrations for each Q_{DGI} value. So, for every reach there was a distribution of Q_{DGI} values with nine associated solute concentrations. Each set of associated solutes were then used in PHREEQC to establish DGI SI_C, SI_D, and P_{CO2} (Parkhurst & Appelo, 2013). These calculations assumed DGI had the same temperature and pH as the median spring values

during the corresponding synoptic sampling event. This assumption is reasonable because DGI are, by definition, coming from groundwater pathways.

3.5 DGI Comparison to Springs or River Samples

Typically, hydrologic studies in karst watersheds focus on springs or streams (Liu et al., 2021). Therefore, data and analyses of hydrologic connectivity are abundant for streams and springs in karst watersheds (Olarinoye et al., 2020). If DGI could be related or compared to either streams or springs, then information about these might reasonably be extrapolated to DGI.

This led to a principal component analysis (PCA) on streams, springs, and DGI using saturation indices, solute concentrations, and solute isotope ratios. PCA is widely used to examine groundwater chemistry because it supports meaningful visualization of a multitude of chemical features and identifies the chemical features which explain the most variation amongst sampled waters (e.g., De la Torre et al., 2020; Dossi et al., 2007; Lastennet & Mudry, 1997). By identifying the features which explain the most variation amongst sampled waters, PCA can help classify the flow and potentially identify distinct end members (Doctor et al., 2006; Long & Valder, 2011). Here chemical features were scaled to make every feature distribution have a mean of 0 and standard deviation of 1, using Scikit-learn's StandardScaler class (Pedregosa et al., 2011). Then, using Scikit-learn's PCA class (Pedregosa et al., 2011) to determine the principal components, the DGI, spring, and stream samples were plotted on the data's first two principal components. Additionally, the chemical features were plotted on the first two principal components to show the variation explained by the features.

3.6 Karst vs. Matrix Groundwater Sources

Karst and matrix springs are fed by flowpaths which are likely going to be affected differently by climate change and the associated shift from snow to rain in mountainous areas. Thus, identifying karst and matrix springs in a watershed is important to understanding the impact of climate change.

Conducting PCA on the collective spring datasets from both synoptic sampling events helped distinguish which springs were fed by karst or matrix flowpaths. Following the same procedure as above for PCA, the spring data were examined (Pedregosa et al., 2011). Since this PCA did not include DGI, which has limited known solute concentrations and solute isotope compositions, this PCA could utilize more of the data collected during the sampling efforts. Major ion concentrations, P_{CO2}, SI_D, SI_C, pH, water temperature, discharge, water and solute isotope ratios, dissolved oxygen concentration, and river distance for each site were considered in the PCA. This chemical feature set also included the change between the measured value of each constituent from June to October. The differences between June and October concentrations were included because Shuster & White (1971) found variation of some constituent concentrations were more indicative of karst versus matrix springs than the actual constituent concentrations.

The clusters of springs produced by the PCA were classified as karst and matrix based on prior information about springs. This prior information included chemical variability in springs, past tracer studies, geologic structure at the spring outlet, and spring hydrographs. This discrete classification of springs can then be extended to quantify the karst and matrix components of DGI.

3.7 DGI Sources and Contribution

Upon classifying karst and matrix springs with the larger chemical dataset, DGI can be compared to the springs to see if DGI is more like the karst or matrix springs. To do this, another PCA was conducted on spring data using solute concentrations: Na^{+}, Ca^{2+}, K^{+}, Mg^{2+}, Cl^{-}, SO_4^{2-}, Alkalinity as $CaCO_3$, U, Sr; isotope ratios: $^{87}Sr/^{86}Sr$, $^{234}U/^{238}U$; and saturation indices: SI_C, SI_D, and P_{CO2}. Then, the DGI chemical data was transformed into this PCA space.

Although DGI may plot near one group of springs, either karst or matrix, DGI are probably not sourced entirely from karst or matrix flowpaths, but likely comprise a component of each. Thus, quantifying the karst and matrix component of DGI gives a more complete understanding of DGI and its resilience to climate change.

Two-solute balances can be used to quantify the contributions of karst (DGI-1) and matrix (DGI-2) components. Distinct solute concentration ranges for both components (DGI-1, DGI-2) provide the least ambiguous estimations of Q_{DGI-1} and Q_{DGI-2}. To identify distinguishable solute concentration ranges between the karst (DGI-1) and matrix (DGI-2) components, the distributions of karst and matrix springs were compared for each solute based on the distinction of matrix and karst from the collective PCA. The solutes with distinguishable solute concentration ranges between karst and matrix springs were used in the two-solute balances.

As with the one-solute balances, the largest net groundwater loss (1 cms) provided a cap on the acceptable Q_{DGL} values in the two-solute balances. A_{DGI-1}, A_{DGI-2}, B_{DGI-1}, and B_{DGI-2} ranges were established based on the distributions of karst and matrix springs. Sampling 20 times from an assumed uniform distribution for each of the

components' solute concentrations (A_{DGI-1}, B_{DGI-1}, A_{DGI-2}, B_{DGI-2}), 160,000 two-solute balances were completed for each reach in each sample period. Results using the OI assumptions were evaluated.

4 RESULTS

4.1 Flow, One-Solute, and One-Isotope Balance Application

The one-solute and one-isotope balances reveal spatial variation in DGI for both high and low flow seasons (Fig. 6, Fig. 7), with variation in quantity and chemistry between seasons (Fig. 8). In June, Q_{DGI} varies along the whole river (Fig. 6A). There does not appear to be a relationship between river distance and Q_{DGI}, except several of the upper reaches (R22, R24, R26) have Q_{DGI} greater than the flow in the river. This is consistent with the significant role of groundwater in the area, exhibited by the numerous springs in the upper basin (Fig. 1). Additionally, surface runoff from lingering snowpack at high elevations could have augmented the flow in these upper reaches.

In June, the reach-scale Q_{DGI} estimated via the one-solute balances are relatively consistent when comparing the results using different solutes (Fig. 6A). There are exceptions where some of the one-solute balances predict a tighter range for Q_{DGI} than other solutes (e.g., Na^+ in R21). There are not any solutions for most one-solute balances in R5, suggesting the influence of the assumed 1 cms Q_{DGL} cap and/or inappropriate solute ranges for this DGI water source.

Some reaches are not sensitive to C_{DGI} (e.g., R20 and R18), meaning DGI could have a wide range of solute concentrations, while others are very sensitive (e.g., R17 and R4) (Fig. 6B). Typically, I_{DGI} are more sensitive than C_{DGI} and have a much narrower range (Fig. 6B), suggesting I_{DGI} are well defined relative to the range of sampled isotope ratios in the watershed. Except in R26, R25, and R24, where the DGI $^{87}Sr/^{86}Sr$ is relatively high, DGI $^{87}Sr/^{86}Sr$ is consistent throughout the watershed (Fig. 6B). The DGI

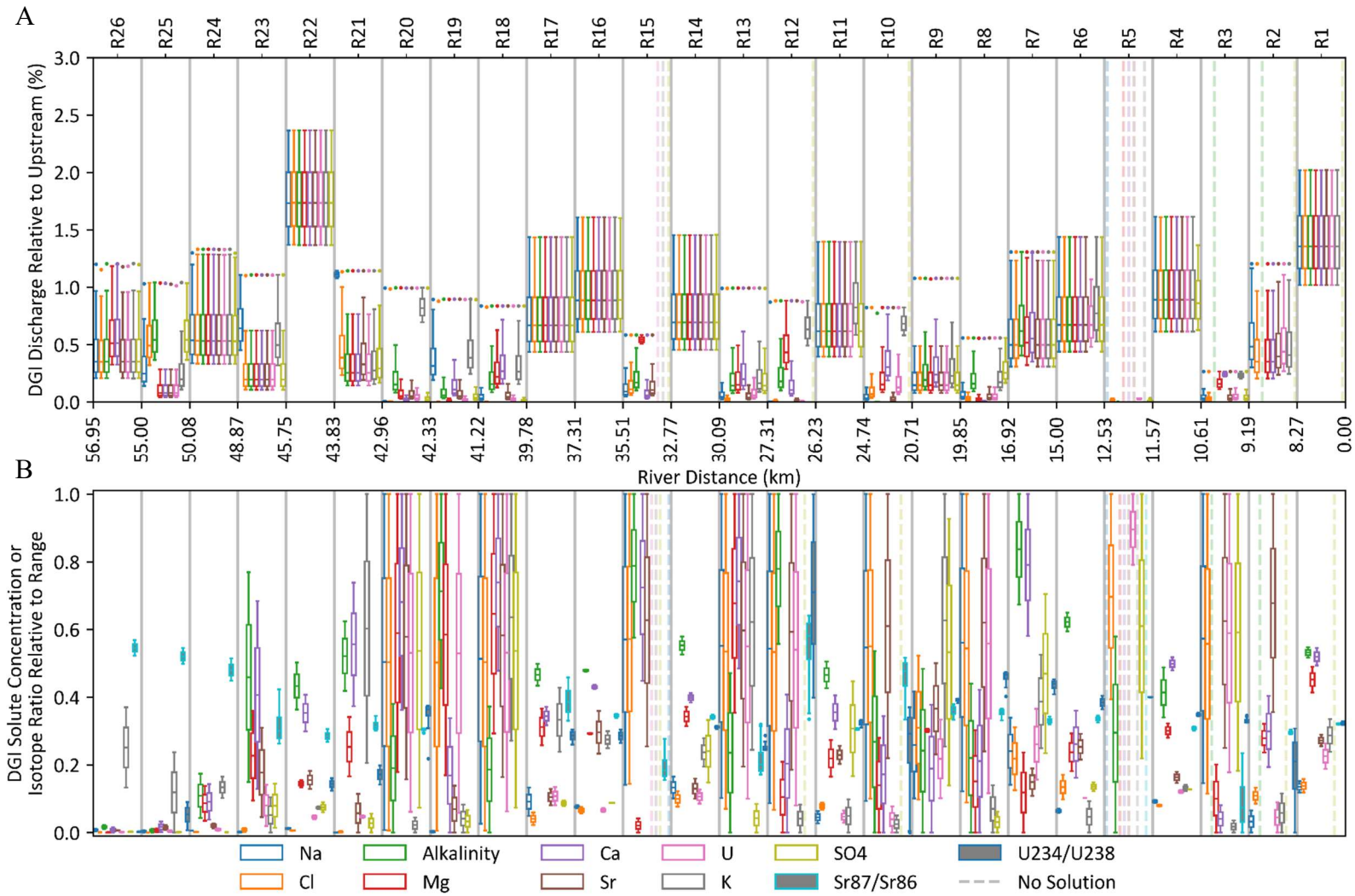

Fig. 6. The estimated DGI discharge based on the nine one-solute balances in June, relative to the discharge at the river site on the upstream side of the reach (A). The solute concentrations or isotope ratios relative to the range of samples measured throughout the watershed in June (B).

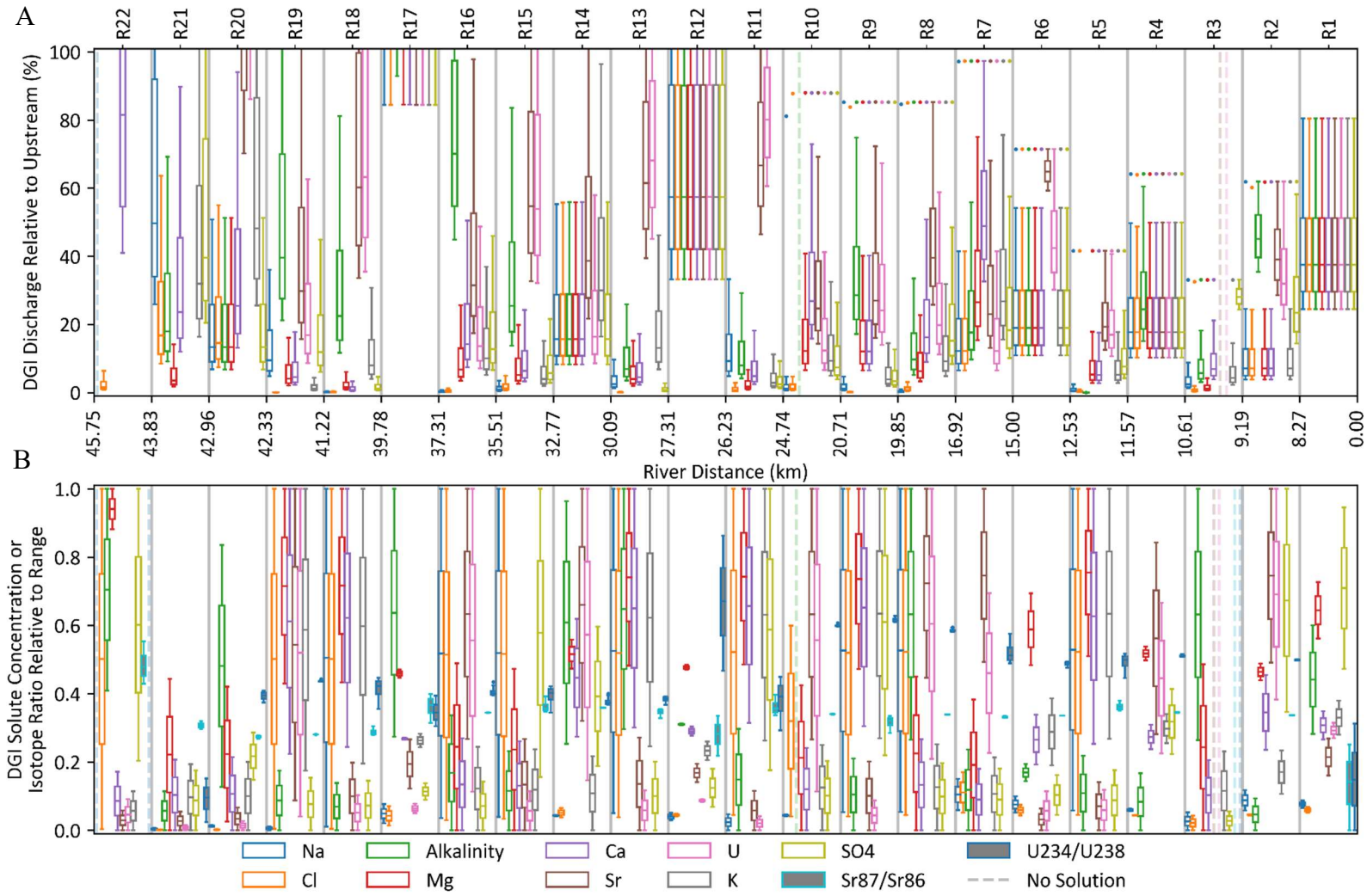

Fig. 7. The estimated DGI discharge based on the nine one-solute balances in October, relative to the discharge at the river site on the upstream side of the reach (A). The solute concentrations or isotope ratios relative to the range of samples measured throughout the watershed in October (B).

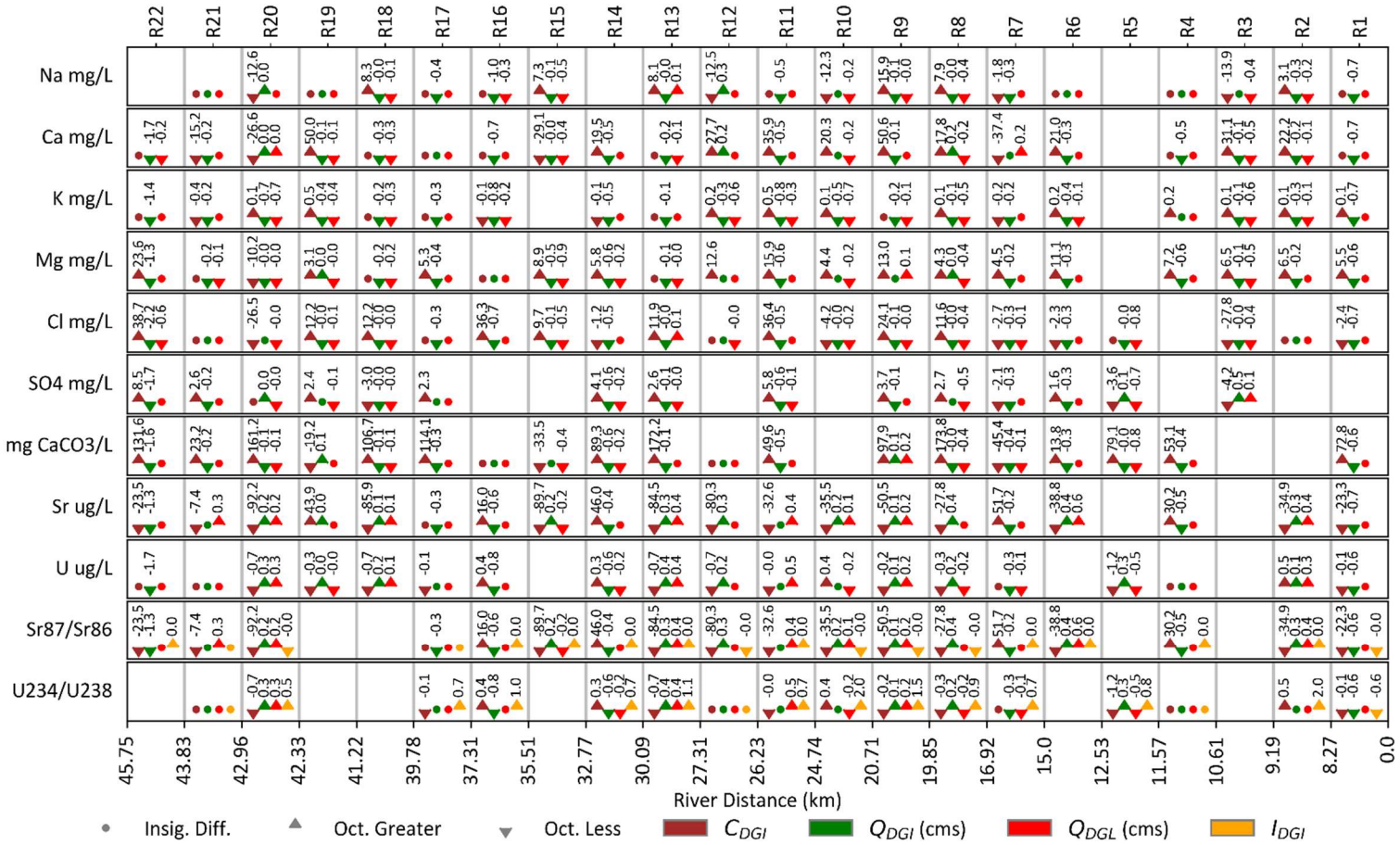

Fig. 8. Summary of results of Mann Whitney U tests between the June and October DGI estimations based on the one-solute balances. The brown, green, red, and yellow icons represent the relationship between June and October C_{DGI}, Q_{DGI}, Q_{DGL}, and I_{DGI}, respectively. The triangle pointing upwards means the solution to the one-solute balance in October is, with 99% confidence, greater than the solution to the one-solute balance in June. The triangle pointing downwards means the solution to the one-solute balance in October is, with 99% confidence, less than the solution to the one-solute balance in June. The circle means there is no statistically significant difference between the June and October solutions.

$^{234}U/^{238}U$ increases downstream until R8 and then decreases to R2 (Fig. 6B). All the DGI solutes have low concentrations in R26-R24, probably because DGI is likely snowmelt (Fig. 6B). Elsewhere, C_{DGI} are sporadic except for in R16 and R17 where they are approximately the same, indicating they likely represent the same source (Fig. 6B).

Like in June, Q_{DGI} in October lacks any longitudinal trend and shows irregular variability (Fig. 7A). The headwater reach (R22) shows extreme Q_{DGI} relative to the flow in the river (Fig. 7A). The ranges of possible Q_{DGI} relative to the river discharge are much wider than in June (Fig. 7A) since the river discharge is smaller in October. Another explanation for the wider ranges of possible Q_{DGI}, could be that the same maximum Q_{DGL} of 1 cms was used for these balances even though the maximum Q_{NET} in any reach was only 0.32 cms during October. A consistent assumed maximum Q_{DGL} was used to ensure the differences in distributions were due to temporal variability.

In October, the Q_{DGI} estimated by the U and Sr balances are consistently higher than the estimates produced by other one-solute balances (Fig. 7B). C_{DGI} lack any longitudinal trend (Fig. 7B). The longitudinal trend in $^{234}U/^{238}U$ (Fig. 7B) is not as clear as it was in June (Fig. 7B). As in June (Fig. 6B), the DGI $^{87}Sr/^{86}Sr$ is consistent throughout the entire river, but with a different ratio (Fig. 7B).

Directly comparing results from June and October reveals temporal variability (Fig. 8). Broadly, there is lower Q_{DGI} in October, though there are a few exceptions. For example, in R19 and R11 there are indications that Q_{DGI} increases in October. Though less significant, there also appears to be less Q_{DGL} in October, suggesting Q_{DGL} is impacted by stage in some reaches (Fig. 8).

In general, there is an increase in C_{DGI} from June to October, though R19 and R7 have a decrease in more solutes' concentrations (Fig. 8). Many of the reported shifts in C_{DGI} are extreme and are influenced by a significant expansion or reduction in the range of possible C_{DGI} and might not reflect a true shift in C_{DGI} (Fig. 8). For example, if the Na^+ balance solutions have a range of DGI sodium concentrations from 5 mg/L to 7 mg/L in June and from 5 mg/L to 20 mg/L in October, the reported temporal shift would be very large. In this example, the reported temporal shift is possible according to the mass balances, though a consistent DGI Na^+ concentration of 5 mg/L is also possible.

Two DGI solutes, Mg^{2+} and Alkalinity (as $CaCO_3$), increase in almost every reach between June and October. DGI Ca^{2+}, K^+, and SO_4^{2-} are less consistent, but still increase in the majority of reaches with significant changes. DGI Na^+ and Cl^- each increase and decrease in about the same number of reaches. DGI Sr and U decrease in concentration in the majority of reaches with significant changes. Conversely, DGI $^{87}Sr/^{86}Sr$ and $^{234}U/^{238}U$ increase in the majority of reaches with significant changes.

4.2 DGI Comparison to Springs or River Samples

In an effort to understand how these resulting C_{DGI} and I_{DGI} are related to the river or spring solute concentrations and solute isotope ratios, the PCA of the DGI estimates, spring samples, and river samples was completed (Fig. 9). The PCA shows DGI estimates and spring samples are more closely related to each other than they are to the river samples (Fig. 9B, Fig. 9D). Springs samples have the most variation (Fig. 9B, Fig. 9D), so they likely have greater influence on the PCA. The spring samples are distinct from the river samples, except there are a few spring samples which plot within or very near the cluster of river samples in both seasons (Fig. 9B, Fig. 9D).

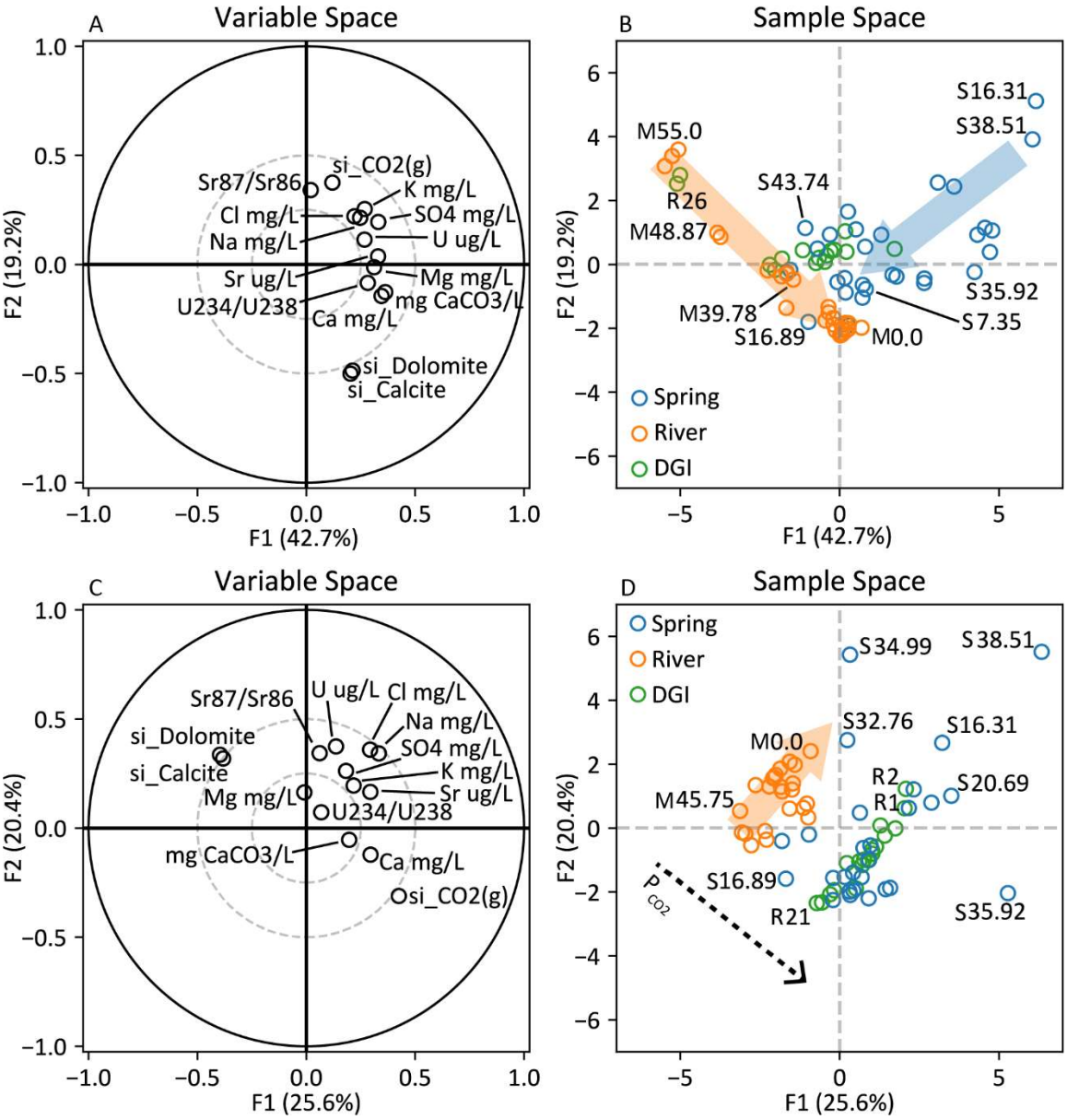

Fig. 9. Results of the June (A & B) and October (C & D) PCA of spring and river samples and DGI estimates. June variables plotted on the first two principal components (A). June samples plotted on the first two principal components (B). The orange arrow indicates the trend of upstream to downstream for the river samples (B). The blue indicates the trend of decreasing solute concentration in the spring samples (B). October variables plotted on the first two principal components (C). October samples plotted on the first two principal components (D). The orange arrow indicates the trend of upstream to downstream for the river samples (D). The black dashed line indicates the trend of decreasing P_{CO2} (D).

In June, the river and spring samples seem to show a mixing relationship (Fig. 9B). The river sample line starts (on the upper left) with samples high in the watershed, derived from snowmelt with low solute concentrations, and trends toward the samples lower in the watershed with slightly higher concentrations. The spring sample line is less defined but starts (on the upper right) with springs with high solute concentrations and presumably longer residence times and then trends towards the large low concentration springs in the watershed which coincide with the lower watershed river samples. Some DGI estimates plot near the upper watershed river samples, dominated by snowmelt, the rest trend towards the low solute concentration springs.

In October, the river samples do not seem to have a mixing relationship with springs (Fig. 9D). Instead, the river samples plot almost entirely in the upper left quadrant and show a trend from upper to lower watershed as the points move up and to the right (Fig. 9D). This variation is strongly described by Cl^- and Na^+ (Fig. 9C). The DGI estimates follow the same trend described by Cl^- and Na^+, from upper to lower watershed, but plot in the middle of the spring sample points (Fig. 9D). The variables which differentiate river samples from DGI estimates and spring samples are P_{CO2}, SI_C, and SI_D (Fig. 9C).

4.3 Saturation Indices

Since P_{CO2}, SI_C, and SI_D are the variables which describe the most variation in springs, DGI, and rivers for both sample periods (Fig. 9A, Fig. 9C), looking at them exclusively is informative (Fig. 10). The DGI estimate and spring sample cluster is the most apparent in October in both the SI_C vs SI_D (Fig. 10B) and P_{CO2} vs SI_D plot (Fig. 10D). There are two springs which plot near the river samples, S19.56 and S39.33 (Fig.

10B, Fig. 10D). These two springs may plot so near the river samples because they were sampled far enough from the spring outlet to allow discharge to equilibrate with the atmosphere and lose some CO_2 to the atmosphere, thus decreasing P_{CO2} and increasing the SI_C and SI_D.

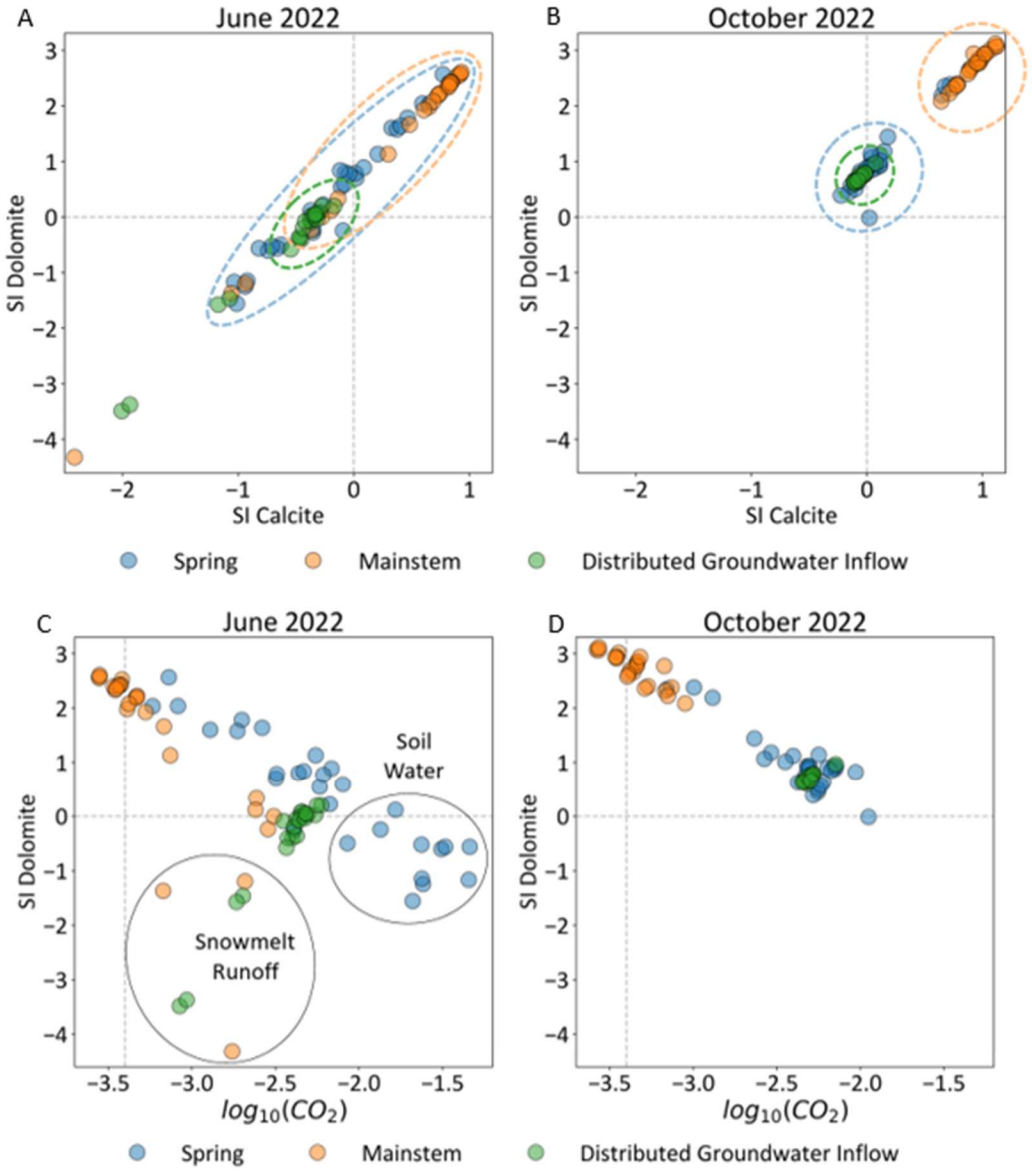

Fig. 10. Comparison of saturation indices for spring and river samples and DGI estimates for June (A and C) and October (B and D). The colored, dashed ovals are drawn to emphasize the clustering of the corresponding samples (A and B). Black ovals are drawn to show unique clusters of data points for June (C).

In June, the distinction is much less clear; however, most river samples show a higher saturation index and lower P_{CO2} than most spring samples and DGI estimates (Fig. 10A, Fig. 10C). The river samples with low saturation indices are from the upper watershed where streamflow is mostly made up of water with extremely low solute concentrations (Fig. 10A, Fig. 10C). Another factor blurring the distinction between spring and river water could be that many springs are very turbulent when surfacing in June, so they immediately entrain air and degas CO_2. Accounting for these factors, DGI estimates look mostly like springs even in June (Fig. 10A, Fig. 10C), but clearly in October (Fig. 10B, Fig. 10D).

4.4 Karst vs. Matrix Groundwater Sources

After establishing DGI are more like springs, we partitioned the springs (Fig. 11B). There are no variables that explain large portions of the variance between all springs, so a PCA considering all the variables simultaneously revealed trends that individual variables could not (Fig. 11). In a PCA exclusively of spring samples and all the data collected for them in these two sampling events, there is a spectrum between karst and matrix springs (Fig. 11B).

The first principal component, or the x axis, is a spectrum from karst on the left to matrix on the right (Fig. 11). This classification is based on several springs on either side of the PCA plot (Fig. 11B) which have been classified as predominantly karst- or matrix-fed based on past research (Neilson et al., 2018; Spangler, 2001). There are no outstanding variables which describe the most variation along the first principal component (Fig. 11A). The water temperature in June and the change in U concentration between seasons have the largest magnitude in the first component direction (Fig. 11A).

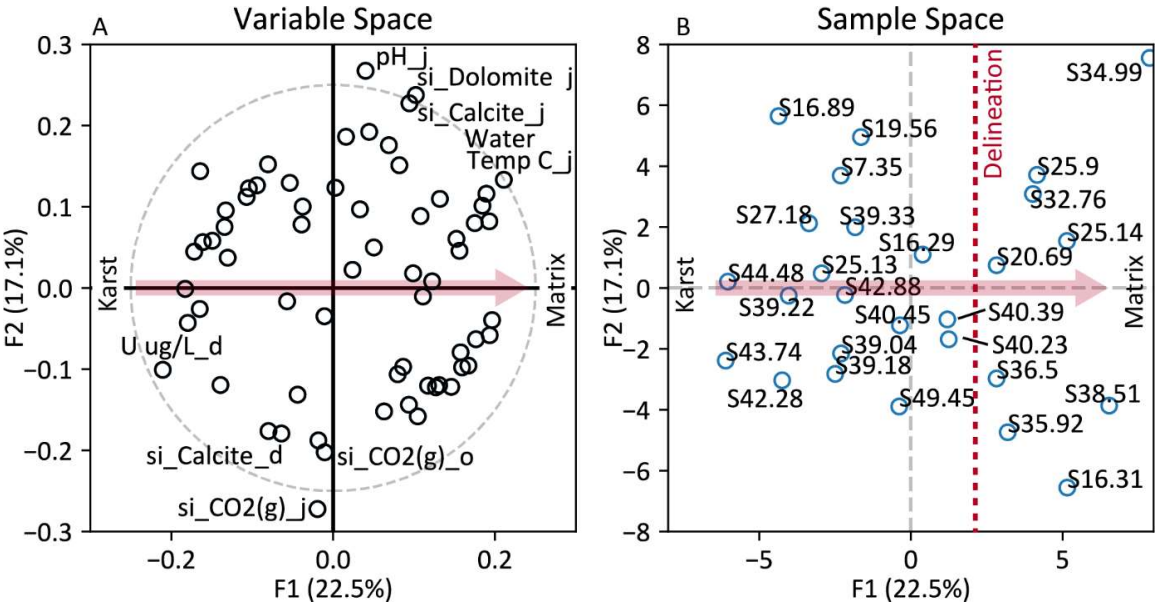

Fig. 11. Spring PCA with all data, for both seasons, including the change of each chemical constituent between seasons. The red arrow (A and B) indicates the spectrum from karst to matrix. Variables plotted on the first two principal components (A). Spring samples plotted on the first two principal components (B). The red dashed line represents the delineation used in the rest of analyses between what is considered karst and matrix (B).

However, dozens of other variables have very similar magnitudes (Fig. 11A). P_{CO2}, SI_C, SI_D, and pH all seem to explain a large portion of variance in the direction of the second component (Fig. 11A); however, this is of less interest than distinguishing between karst and matrix type springs.

4.5 DGI Sources and Contribution

Once the springs were partitioned, the DGI were compared to the springs to see if DGI is more like karst or matrix springs (Fig. 12B, Fig. 12D). In both seasons, the DGI is more like karst springs (Fig. 12B, Fig. 12D). Since less chemical information is known or estimated for DGI, fewer variables were included in the PCA. Despite this change, a principal component in each season distinguishes karst from matrix springs as in the PCA

which separated the springs (Fig. 12B, Fig. 12D). The variables explaining the most variation on the axis which distinguishes karst and matrix springs in June (Fig. 12A) and October (Fig. 12C) are Sr, SO_4^{2-}, K^+ and Na^+, Ca^{2+}, Sr, respectively.

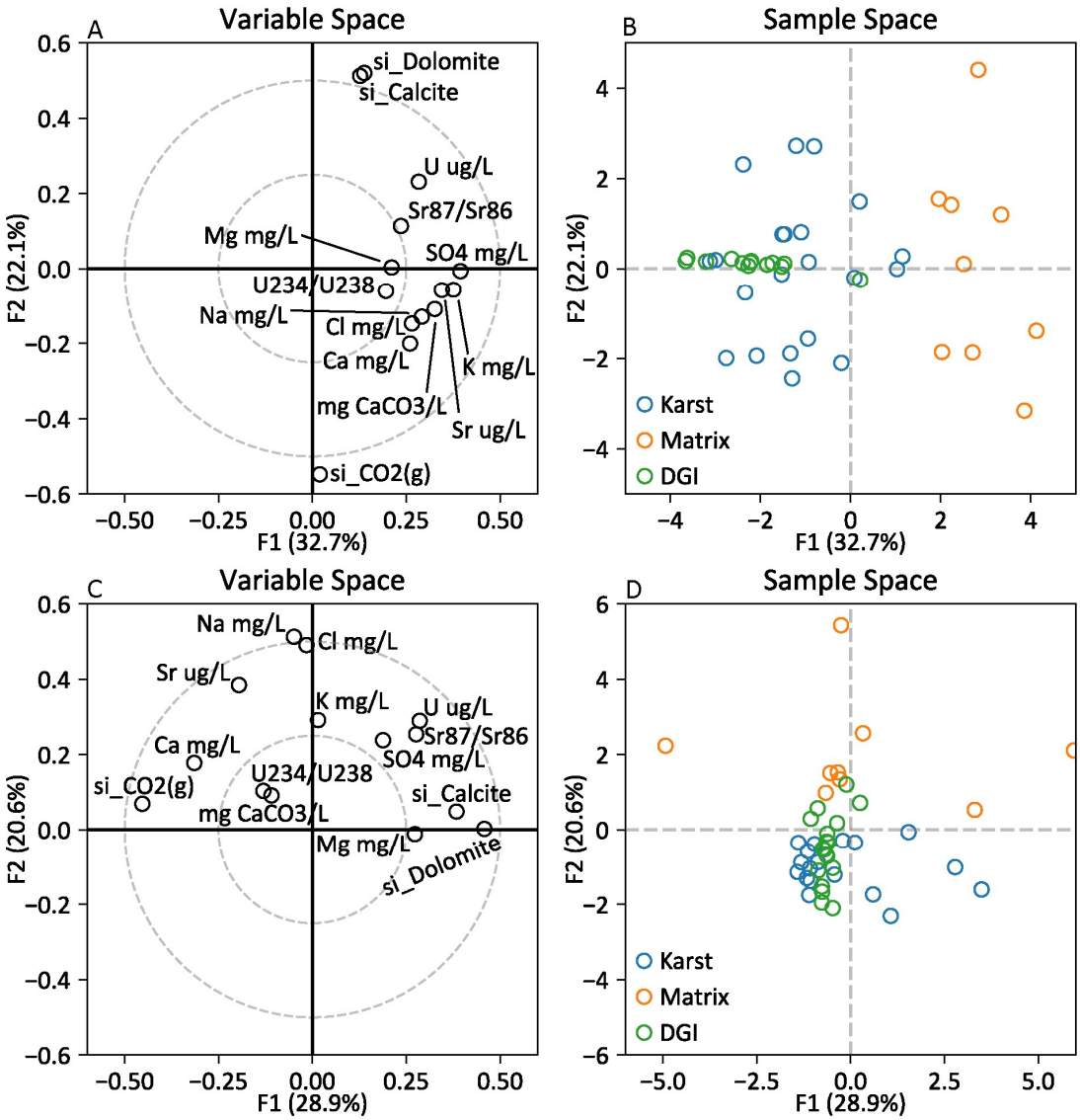

Fig. 12. Spring PCA results with only the chemical features which are known for DGI (concentrations: Na^+, Ca^{2+}, K^+, Mg^{2+}, Cl^-, SO_4^{2-}, Alkalinity (as $CaCO_3$), U, Sr; isotope ratios: $^{87}Sr/^{86}Sr$, $^{234}U/^{238}U$; saturation indices: SI_C, SI_D, P_{CO2}). June variables plotted on the first two principal components (A). June spring samples and DGI estimates plotted on the first two principal components (B). October variables plotted on the first two principal components (C). October spring samples and DGI estimates plotted on the first two principal components (D).

The DGI estimates have the most spread in the direction which distinguishes karst and matrix (Fig. 12B, Fig. 12D). DGI estimates are uniform in the other direction, mainly controlled by SI_C, SI_D, and P_{CO2} (Fig. 12A, Fig. 12C). Some of the DGI is more extreme on the karst spectrum than karst springs during June, and in general the DGI appears much more like karst than matrix (Fig. 12B). In October, the saturation indices are most variable and they take over the first principal component, so the second principal component becomes the karst to matrix distinguishing component (Fig. 12D). The DGI plot closer to the matrix side of the spectrum relative to June, but the distinction between karst and matrix is still clear and the DGI would still be classified as karst (Fig. 12B, Fig. 12D).

After classifying springs as either karst or matrix, the observed chemical distributions of karst and matrix springs were compared (Fig. 13). In both seasons, for almost every constituent, the matrix spring distributions have a larger median value than the karst spring distributions (Fig. 13). The exception are the saturation indices (SI_C, SI_D) and P_{CO2} of which the karst and matrix spring distributions have similar medians (Fig. 13). The $^{87}Sr/^{86}Sr$ ratio and Na^+, K^+, Cl^-, SO_4^{2-}, Sr, and U concentrations reveal distinct karst and matrix spring distributions (Fig. 13).

Assuming the DGI have chemically similar karst and matrix components, the solute ranges of karst and matrix springs are applicable to two-solute balances for quantifying karst and matrix contributions (Fig. 14, Fig. 15). The solutes with distinct ranges are most useful for this analysis because they provide less ambiguous results (i.e., the DGI karst component is less likely to be mistaken for the DGI matrix component and

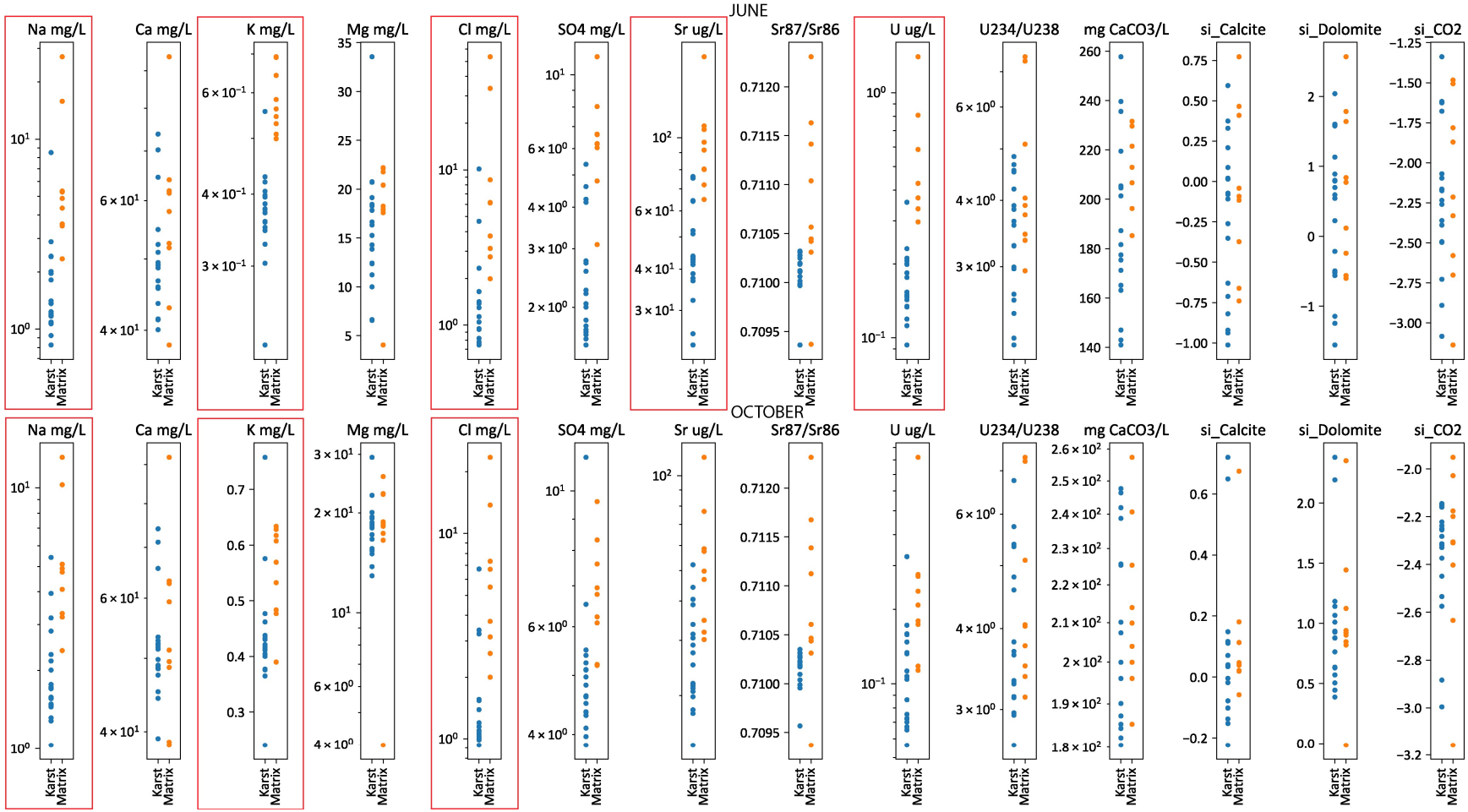

Fig. 13. The karst and matrix spring distributions of the solutes, isotope ratios, and saturation indices in June and October. Including only the solutes, isotope ratios, and saturation indices which can be estimated for DGI. The highlighted solutes were the solutes ultimately used in the two-solute balances.

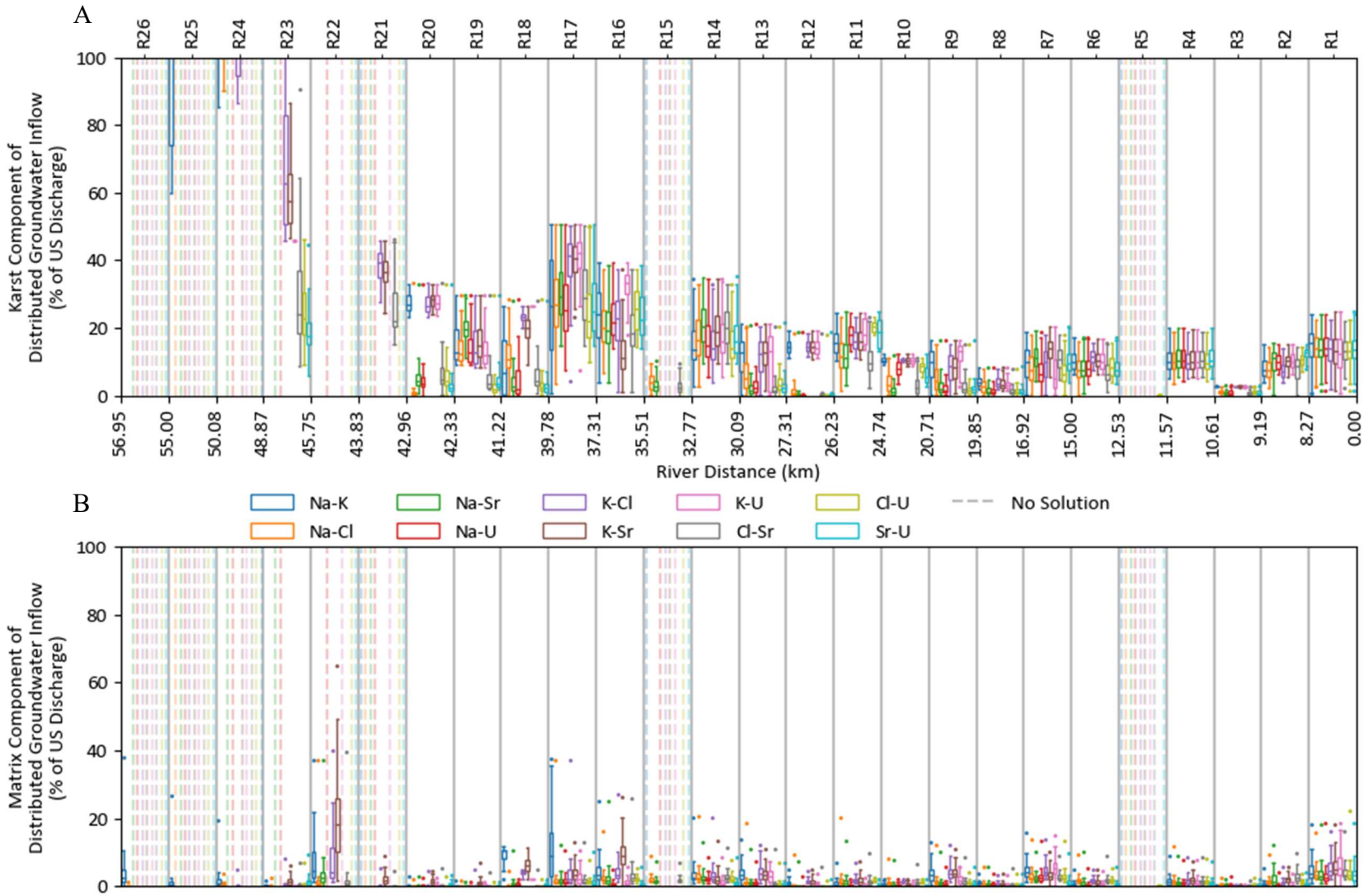

Fig. 14. Two-solute balances in June. Karst contributions, relative to the upstream discharge, as estimated by 10 two-solute balances (A). Corresponding matrix contributions as estimated by the two-solute balances (B).

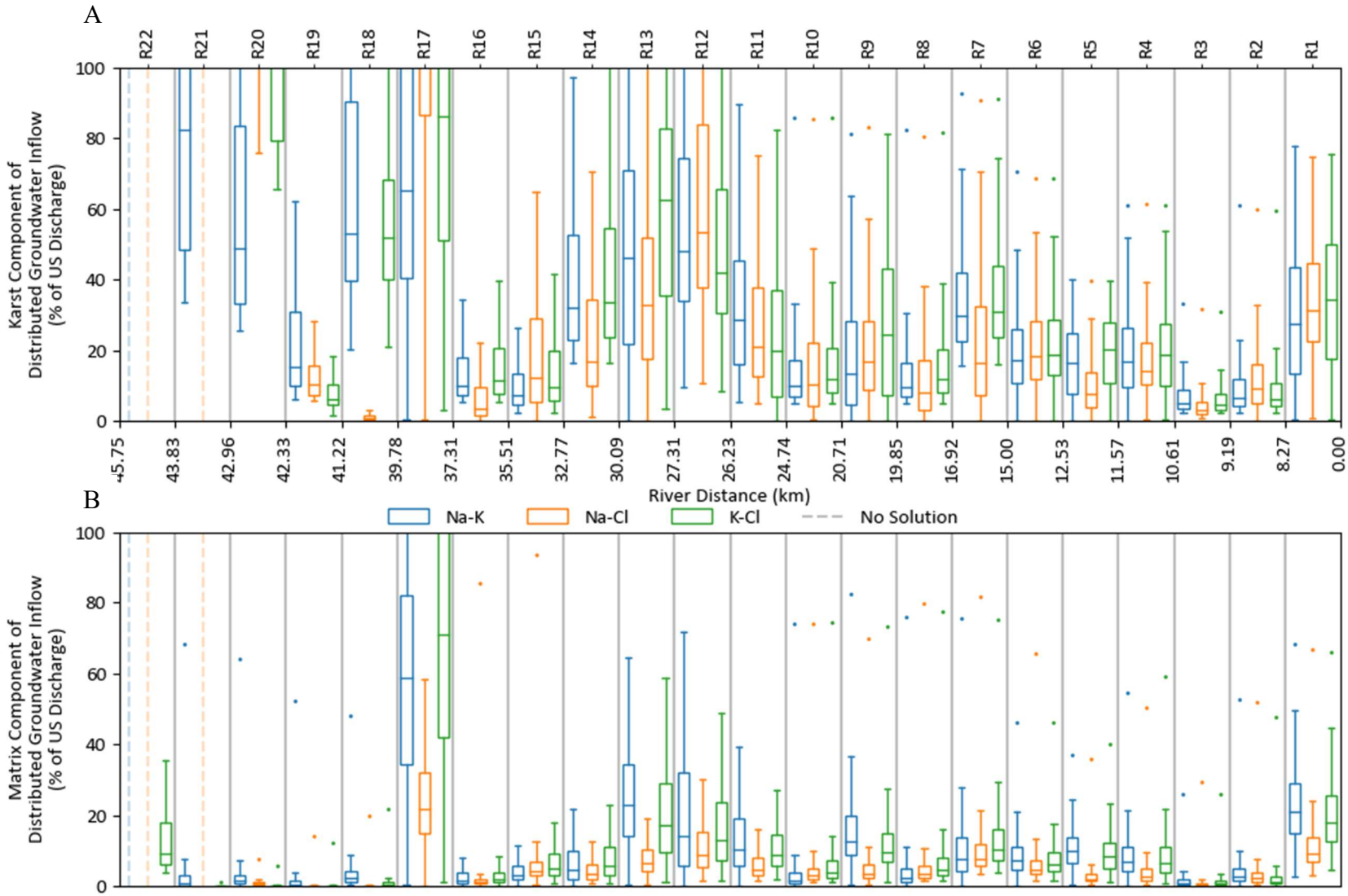

Fig. 15. Two-solute balances in October. Karst contributions, relative to the upstream discharge, as estimated by three two-solute balances (A). Corresponding matrix contributions as estimated by the two-solute balances (B).

vice versa). Therefore, Na^+, K^+, Cl^-, SO_4^{2-}, Sr, and U concentrations were initially used for two-solute mass balances.

Several of the initial solutes selected for the two-solute balances were excluded from one or both seasonal two-solute balances. SO_4^{2-} was excluded from the June balances since several of the upper reaches did not have solutions because DGI SO_4^{2-} concentrations were lower than the lowest concentration observed in karst springs and the upstream site of R1 SO_4^{2-} measurement was erroneous. SO_4^{2-} was also excluded from the October balances because a large karst spring with an extraordinarily high concentration encompasses the entire matrix SO_4^{2-} distribution (Fig. 13). Sr and U were excluded from the October balances, because they consistently overpredicted Q_{DGI} in the one-solute balances (Fig. 7).

In the end, Na^+, K^+, Cl^-, Sr, and U were used in June two-solute balances and Na^+, K^+, and Cl^- were used in October two-solute balances. Every unique pair of solutes was used: 10 pairs for June and 3 pairs for October. The results for June two-solute balances reveal a cumulative karst contribution ranging from 83.5% to 91.9% of all DGI (Fig. A 1). The results for October two-solute balances reveal a karst contribution ranging from 63.3% to 76.6% of cumulative DGI (Fig. A 2).

Although the karst fraction is consistent between two-solute balances, the discharge value of the cumulative karst component of DGI is highly variable in June (Fig. A 1). The cumulative karst discharge varies from 8.25 cms to 15.63 cms in June (Fig. A 1), but only from 3.54 to 5.05 cms in October (Fig. A 2). The four largest estimates of karst discharge in June result from two-solute balances including K^+ (Fig. A 1). The karst K^+ concentration range is extended due to an outlying spring (S16.89) with extremely

low K^+ concentration (Fig. 13). This extended range is resulting in an overestimation of karst contributions. Excluding the estimates that use K^+, the karst discharge ranges from 8.25 cms to 11.55 cms (Fig. A 1). Clearly, the percent karst contribution decreases between June and October, but the absolute magnitude is unclear due to the large range in possible karst discharges in June.

The cumulative matrix fraction of DGI increases between June and October (Fig. A 1, Fig. A 2). The cumulative matrix discharge is steady relative to the karst discharge, but the percent contribution increases as karst contributions decrease after the bulk of the snowmelt recharge has drained from the conduits. The June matrix discharge ranges from 0.73 cms to 3.0 cms including K^+ balances or 1.66 cms excluding K^+ balances (Fig. A 1). The October matrix discharge ranges from 1.08 to 2.33 cms (Fig. A 2).

The clearest spatial trend, apparent in both seasons, is the upper reaches have nearly no matrix contributions until about R19 (Fig. 14, Fig. 15). Those upper reaches have significant karst contributions relative to the river discharge. These findings are supported by the findings of the one-solute balance. The cumulative karst and matrix DGI are approximately linear, but increase more towards the outlet of the watershed (Fig. A 1, Fig. A 2). This means there are greater matrix and karst discharge lower in the watershed, which suggests the downstream DGI contributions are supported by larger groundwater basins with more complex flowpath distributions.

In June, there are two reaches (R5, R15) which do not have solutions for most of the two-solute balances (Fig. 14). This is consistent with the one-solute balances (Fig. 6), which suggests one or both ranges iterated through for the karst or matrix component were not appropriate or the maximum Q_{DGL} of 1 cms was inappropriate. The lack of

results in R21, R24, R25, and R26 are probably due to dilute snowmelt entering the river that does not fall in the range of karst or matrix.

5 DISCUSSION

Incremental mass and flow balances provide the ability to quantify ground- and surface water interactions and inform a chemical equilibrium model to estimate DGI saturation indices that provide a more comprehensive understanding of DGI water-rock interaction. Extending the mass balances to solute isotope ratios at reach scales, with the mass and flow balances, provide a spatial, high-resolution perspective on the sources of DGI because isotope ratios are natural tracers (e.g., Bullen & Kendall, 1998; Paces & Wurster, 2014).

The observed spatial variability in Q_{DGI} is indicative of karst (Fig. 6A, Fig. 7A). As suggested by Neilson et al. (2018), large inflows in a reach adjacent to a reach with large losses suggest connections to fracture networks. Relative Q_{DGI} is much higher in the upper watershed, likely due to snowmelt augmenting the river via surface overland flow or shallow soil flow in June (Fig. 6A). This suggestion is also supported by the relatively high $^{87}Sr/^{86}Sr$ ratios in the upper reaches probably derived from dust on or in the snow (Carling et al., 2020)(Fig. 6B). There is also relatively high Q_{DGI} in the upper reaches during October, though the river initiation is lower in the watershed later in the summer (Fig. 7A). Since DGI cannot be mistaken for snowmelt or overland flow during October, the river must be sustained by springs and significant DGI in these areas.

The overall decrease in Q_{DGI} between high and low flow seasons was expected because the watershed is snow-dominated and snowmelt influences were still present in June, particularly high in the watershed (Fig. 8). The general decrease in Q_{DGL} indicates its relationship to stage in the river as opposed to available void space in the karst aquifer

(Fig. 8). R12 shifted from net losing in June to net gaining in October suggest delayed residence times or shifts in flowpaths.

The DGI $^{234}U/^{238}U$ ratio spatial trend suggests increasing water-rock interaction downstream until R8 (Fig. 6B, Fig. 7B). Aside from the upper reaches in June, the $^{87}Sr/^{86}Sr$ ratio is starkly consistent and uniform suggesting a dominant and consistent carbonate-bedrock influence year-round (Fig. 6B, Fig. 7B). The DGI $^{87}Sr/^{86}Sr$ ratio increases during low flow season and is accompanied by lower DGI Sr concentrations (Fig. 8), consistent with an increase of flow paths interacting with silicate bedrock (McNutt, 2000). The other DGI solute concentrations generally increase during low flow seasons supporting the hypothesis of increased matrix flow (Fig. 8). This study is limited to observing general intra-annual shifts but does provide higher spatial resolution with a larger suite of solutes than previous studies (Lachmar et al., 2021; Neilson et al., 2018).

The estimated DGI chemistry was compared to both river and spring water (Fig. 9). This analysis suggests DGI is similar to spring water (Fig. 9B, Fig. 9D). This finding is almost entirely based on saturation indices (Fig. 10). This finding is very sensitive to pH (Minvielle et al., 2015) and temperature which was assumed to be the median spring pH and temperature for the given event. The springs in June have more variable saturation indices than river water or DGI (Fig. 10). This may be because the springs have varied flushing effects, soil water effects, and limited interactions with rock. In June, the relationship between DGI, river, and spring water demonstrates mixing overland or shallow soil snowmelt, snowmelt through karst conduits, and longer residence time or matrix groundwater (Fig. 9B).

To further get at the DGI karst versus matrix contributions, the suite of spring chemical data collected in this study was used to distinguish springs and establish solute concentration ranges for karst and matrix type water (Fig. 13). Although the ranges are not perfectly distinct, matrix spring distributions consistently have higher medians than the karst distributions (Fig. 13). This is expected because the matrix springs have longer residences times and more rock surface area that leads to more water-rock interaction and higher solute concentrations. The similar median P_{CO2} between karst and matrix springs (Fig. 13) suggests each type have limited interaction with the atmosphere after flowing through soils enriched in CO_2 and/or the subsurface fracture zones have elevated P_{CO2}.

The slightly overlapping solute concentration ranges between karst and matrix along with the temporal shift in solute concentration ranges between seasons are due to the fact that karst and matrix are not two distinct end members, but create a continuum (Fig. 11, Fig. 13) (Worthington, 1999). The most important difference between karst and matrix springs in the context of climate change is residence time. Since springs have a large distribution of residence times (Bethke & Johnson, 2008; Ozyurt, 2008) and the residence time is difficult to measure, we have used spring solute concentration and isotope ratio as an indication of residence times.

The two-solute balances suggest a substantial portion of DGI is sourced through karst conduits (Fig. 14, Fig. 15). This finding is consistent with the findings of Neilson et al. (2018) and Lachmar et al. (2021). Beyond this general finding, there are differences between studies which may be a result of methodological differences, hydrologic conditions at the time of sampling (Fig. A 3), and/or the resolution of sampling. First, Neilson et al. (2018) did not observe a spatially consistent increase in DGI matrix

fraction from June to August flow periods in 2015. In contrast, this study found the matrix component of DGI increased significantly later in the baseflow period (October). Second, Lachmar et al. (2021) observed a larger matrix fraction in three springs than this study (Fig. 14, Fig. 15) and Neilson et al. (2018). However, it should be noted that Lachmar et al. (2021) partitioned "matrix" as decadal water and flow through solution-enhanced pore space. Despite these differences all studies emphasize the karst component of springs or DGI, both of which sustain river flow throughout the year.

The large fraction of river flow sustained by karst conduits has implications for water quality and watershed resiliency to climate change. The prevalence of karst inflow suggests vulnerability to pollution. The short residence times of karst inflows and their correlation to snowmelt imply that when snowmelt dynamics shift, or precipitation all together shifts from snow to rain, the river dynamics and water supply will change. More study is required to predict the effects of shifts from snow to rain; however, this study highlights the impact will be apparent not only in springs, but also in the DGI contributions to streamflow.

6 CONCLUSION

Here we computed various high-resolution reach-scale mass and isotope balances throughout a highly karstified, mountainous watershed during runoff and baseflow conditions in a very dry year. The mass balances revealed spatial, temporal, and directional variability in surface-groundwater interaction. Multivariate or principal component analysis of river and spring data along with DGI estimates revealed DGI is chemically similar to springs, implying springs are representative of other large distributed groundwater inflows. Multiple lines of evidence indicate karst conduits and solution-enhanced fractures are the predominant flow paths supplying DGI with an increasing fraction of matrix sourced water during baseflow. The prevalence of karst conduit sourced groundwater in both DGI and springs suggests vulnerability of the entire system to climate change and extended periods of drought.

ENGINEERING SIGNIFICANCE

As the shifts associated with climate change continue to unfold and populations relying on karst aquifers increase, management of karst aquifers will increase in consequence. This study demonstrates the significant magnitude of river exchanges with karst aquifers in addition to inflows from karst springs. In karst watersheds with surface water flows, these distributed groundwater exchanges are likely not trivial. An assessment of aquifer condition includes the consideration of these exchanges to manage these watersheds holistically.

Aside from suggesting the importance of accounting for the quantity of water exchanging between aquifer and river, this study demonstrates the potential for water to enter or re-enter the ground from the river channel. Pollutants spilled in the river can enter and contaminate the aquifer. When developing adjacent to rivers in karst regions, the risk of contaminating surface- and groundwater ought to be evaluated. In the case of the Logan river watershed, there is limited development, but a state highway parallels the river for about 40 km. The transport of substances which could spill during a crash presents a hazard to the water users downstream and possibly the groundwater aquifer.

REFERENCES

Bahr, K. (2016). *Structural and lithological influences on the Tony Grove alpine karst system, Bear River Range, north central Utah* (Master's thesis). Utah State University, Logan, Utah. https://doi.org/10.26076/7acb-98cf

Bailly-Comte, V., Jourde, H., & Pistre, S. (2009). Conceptualization and classification of groundwater–surface water hydrodynamic interactions in karst watersheds: Case of the karst watershed of the Coulazou River (Southern France). *Journal of Hydrology*, *376*(3–4), 456–462. https://doi.org/10.1016/j.jhydrol.2009.07.053

Bakalowicz, M. (2005). Karst groundwater: A challenge for new resources. *Hydrogeology Journal*, *13*(1), 148–160. https://doi.org/10.1007/s10040-004-0402-9

Barnett, T. P., Adam, J. C., & Lettenmaier, D. P. (2005). Potential impacts of a warming climate on water availability in snow-dominated regions. *Nature*, *438*(7066), 303–309. https://doi.org/10.1038/nature04141

Baudement, C., Arfib, B., Mazzilli, N., Jouves, J., Lamarque, T., & Guglielmi, Y. (2017). Groundwater management of a highly dynamic karst by assessing baseflow and quickflow with a rainfall-discharge model (Dardennes springs, SE France). *Bulletin de La Société Géologique de France*, *188*(6), 40. https://doi.org/10.1051/bsgf/2017203

Bethke, C. M., & Johnson, T. M. (2008). Groundwater age and groundwater age dating. *Annual Review of Earth and Planetary Sciences*, *36*(1), 121–152. https://doi.org/10.1146/annurev.earth.36.031207.124210

Bonacci, O., Oštrić, M., & Roje Bonacci, T. (2018). Water resources analysis of the Rječina karst spring and river (Dinaric karst). *Acta Carsologica*, *47*(2–3). https://doi.org/10.3986/ac.v47i2-3.5182

Brezinski, D. K. (2007). Geologic and anthropogenic factors influencing karst development in the Frederick region of Maryland. *Environmental Geosciences*, *14*(1), 31–48. https://doi.org/10.1306/eg.01050605014

Bullen, T. D., & Kendall, C. (1998). Tracing of weathering reactions and water flowpaths: A multi-isotope approach. In C. Kendall & J. J. McDonnell (Eds.), *Isotope Tracers in Catchment Hydrology* (1st ed., pp. 611–646). Oxford: Elsevier. https://doi.org/10.1016/B978-0-444-81546-0.50025-2

Carling, G. T., Fernandez, D. P., Rey, K. A., Hale, C. A., Goodman, M. M., & Nelson, S. T. (2020). Using strontium isotopes to trace dust from a drying Great Salt Lake to adjacent urban areas and mountain snowpack. *Environmental Research Letters*, *15*(11), 114035. https://doi.org/10.1088/1748-9326/abbfc4

Civita, M. V. (2008). An improved method for delineating source protection zones for karst springs based on analysis of recession curve data. *Hydrogeology Journal*, *16*(5), 855–869. https://doi.org/10.1007/s10040-008-0283-4

Dai, A. (2011). Drought under global warming: a review. *WIREs Climate Change*, *2*(1), 45–65. https://doi.org/10.1002/wcc.81

Doctor, D. H., Alexander, E. C., Petrič, M., Kogovšek, J., Urbanc, J., Lojen, S., & Stichler, W. (2006). Quantification of karst aquifer discharge components during storm events through end-member mixing analysis using natural chemistry and stable isotopes as tracers. *Hydrogeology Journal*, *14*(7), 1171–1191. https://doi.org/10.1007/s10040-006-0031-6

Donovan, K. M., Springer, A. E., Tobin, B. W., & Parnell, R. A. (2022). Karst spring processes and storage implications in high elevation, semiarid southwestern United States. In M. J. Currell & B. G. Katz (Eds.), *Threats to Springs in a Changing World: Science and Policies for Protection, Geophysical Monograph Series* (pp. 35–50). Hoboken, NJ: American Geophysical Union. https://doi.org/10.1002/9781119818625.CH4

Dossi, C., Ciceri, E., Giussani, B., Pozzi, A., Galgaro, A., Viero, A., & Viganò, A. (2007). Water and snow chemistry of main ions and trace elements in the karst system of Monte Pelmo massif (Dolomites, Eastern Alps, Italy). *Marine and Freshwater Research*, *58*(7), 649. https://doi.org/10.1071/MF06170

Dover, J. H. (1995). Geologic map of the Logan 30’x60’ quadrangle, Cache and Rich Counties, Utah and Lincoln and Uinta Counties, Wyoming (U.S. Geological Survey Miscellaneous Investigations Series Map I-2210). U.S. Geological Survey. Retrieved from https://ugspub.nr.utah.gov/publications/misc_pubs/mp-06-8.pdf

Drever, J. (1988). The carbonate system and pH control. In *The Geochemistry of Natural Waters* (3rd ed., pp. 41–68). Upper Saddle River, NJ: Prentice-Hall.

Farics, É., Halász, A., Czigány, S., & Pirkhoffer, E. (2021). Vulnerability mapping of karst springs and its application for the delineation of protection zones (Mecsek Karst, Hungary). *Acta Carsologica*, *50*(2–3). https://doi.org/10.3986/ac.v50i2-3.8583

Faure, G. (1986). Isotope systematics of two-component mixtures. In *Principles of Isotope Geology* (2nd ed., pp. 141–153). New York: Wiley.

Fiorillo, F. (2014). The recession of spring hydrographs, focused on karst aquifers. *Water Resources Management*, *28*(7), 1781–1805. https://doi.org/10.1007/s11269-014-0597-z

Fiorillo, F., Leone, G., Pagnozzi, M., & Esposito, L. (2021). Long-term trends in karst spring discharge and relation to climate factors and changes. *Hydrogeology Journal*, *29*(1), 347–377. https://doi.org/10.1007/s10040-020-02265-0

Ford, D., & Williams, P. (2007). *Karst hydrogeology and geomorphology*. West Sussex, UK: John Wiley and Sons Ltd. https://doi.org/10.1002/9781118684986

Gimeno, L., Sorí, R., Vázquez, M., Stojanovic, M., Algarra, I., Eiras-Barca, J., et al. (2022). Extreme precipitation events. *WIREs Water*, *9*(6). https://doi.org/10.1002/wat2.1611

Glaser, C., Schwientek, M., Junginger, T., Gilfedder, B. S., Frei, S., Werneburg, M., et al. (2020). Comparison of environmental tracers including organic micropollutants as groundwater exfiltration indicators into a small river of a karstic catchment. *Hydrological Processes*, *34*(24), 4712–4726. https://doi.org/10.1002/hyp.13909

Goldscheider, N. (2005). Fold structure and underground drainage pattern in the alpine karst system Hochifen-Gottesacker. *Eclogae Geologicae Helvetiae*, *98*(1), 1–17. https://doi.org/10.1007/s00015-005-1143-z

Goldscheider, N., Chen, Z., Auler, A. S., Bakalowicz, M., Broda, S., Drew, D., et al. (2020). Global distribution of carbonate rocks and karst water resources. *Hydrogeology Journal*, *28*(5), 1661–1677. https://doi.org/10.1007/s10040-020-02139-5

Gremaud, V., & Goldscheider, N. (2010). Climate change effects on aquifer recharge in a glacierised karst aquifer system, Tsanfleuron-Sanetsch, Swiss Alps. In B. Andreo, F. Carrasco, J. J. Durán, & J. W. LaMoreaux (Eds.), *Advances in Research in Karst Media, Environmental Earth Sciences* (pp. 31–36). Springer-Verlag Berlin Heidelberg. https://doi.org/10.1007/978-3-642-12486-0_5

Groten, J., & Alexander, E. (2015). Karst hydrogeologic investigation of Trout Brook. In D. H. Doctor, L. Land, & J. B. Stephenson (Eds.), *Sinkholes and the Engineering and Environmental Impacts of Karst: Proceedings of the Fourteenth Multidisciplinary Conference* (pp. 1–8). Carlsbad, NM: National Cave and Karst Research Institute. https://doi.org/10.5038/9780991000951.1012

Hartmann, A., Gleeson, T., Wada, Y., & Wagener, T. (2017). Enhanced groundwater recharge rates and altered recharge sensitivity to climate variability through subsurface heterogeneity. *Proceedings of the National Academy of Sciences of the United States of America*, *114*(11), 2842–2847. https://doi.org/10.1073/PNAS.1614941114/SUPPL_FILE/PNAS.201614941SI.PDF

Hottelet, C., Braun, L. N., Leibundgut, C., & Rieg, A. (1993). Simulation of snowpack and discharge in an alpine karst basin. In G. J. Young (Ed.), *International Symposium on Snow and Glacier Hydrology: Kathmandu, Nepal. IAHS Publication No. 218.* (pp. 249–260). Oxfordshire, UK: International Association of Hydrological Sciences.

Jódar, J., González-Ramón, A., Martos-Rosillo, S., Heredia, J., Herrera, C., Urrutia, J., et al. (2020). Snowmelt as a determinant factor in the hydrogeological behaviour of high mountain karst aquifers: The Garcés karst system, Central Pyrenees (Spain). *Science of The Total Environment*, *748*, 141363. https://doi.org/10.1016/j.scitotenv.2020.141363

Kalbus, E., Reinstorf, F., & Schirmer, M. (2006). Measuring methods for groundwater-surface water interactions: a review. *Hydrology Earth System Science*, *10*(6), 873–887. https://doi.org/10.5194/hess-10-873-2006

Kaufmann, G., Gabrovšek, F., & Romanov, D. (2014). Deep conduit flow in karst aquifers revisited. *Water Resources Research*, *50*(6), 4821–4836. https://doi.org/10.1002/2014WR015314

Keshavarzi, M., Baker, A., Kelly, B. F. J., & Andersen, M. S. (2017). River–groundwater connectivity in a karst system, Wellington, New South Wales, Australia. *Hydrogeology Journal*, *25*(2), 557–574. https://doi.org/10.1007/s10040-016-1491-y

Khadka, M. B., Martin, J. B., & Kurz, M. J. (2017). Synoptic estimates of diffuse groundwater seepage to a spring-fed karst river at high spatial resolution using an automated radon measurement technique. *Journal of Hydrology*, *544*, 86–96. https://doi.org/10.1016/j.jhydrol.2016.11.013

Klaas, D. K. S. Y., Imteaz, M. A., Sudiayem, I., Klaas, E. M. E., & Klaas, E. C. M. (2020). Assessing climate changes impacts on tropical karst catchment: Implications on groundwater resource sustainability and management strategies. *Journal of Hydrology*, *582*, 124426. https://doi.org/10.1016/j.jhydrol.2019.124426

Klos, P. Z., Link, T. E., & Abatzoglou, J. T. (2014). Extent of the rain-snow transition zone in the western U.S. under historic and projected climate. *Geophysical Research Letters*, *41*(13), 4560–4568. https://doi.org/10.1002/2014GL060500

Knowles, N., Dettinger, M. D., & Cayan, D. R. (2006). Trends in snowfall versus rainfall in the western United States. *Journal of Climate*, *19*(18), 4545–4559. https://doi.org/10.1175/JCLI3850.1

De la Torre, B., Mudarra, M., & Andreo, B. (2020). Investigating karst aquifers in tectonically complex alpine areas coupling geological and hydrogeological methods. *Journal of Hydrology X*, *6*, 100047. https://doi.org/10.1016/j.hydroa.2019.100047

Lachmar, T., Sorsby, S., & Newell, D. (2021). Geochemical insights into groundwater movement in alpine karst, Bear River Range, Utah, USA. *Hydrogeology Journal*, *29*(2), 687–701. https://doi.org/10.1007/S10040-020-02256-1/TABLES/9

Land, L., & Timmons, S. (2016). Evaluation of groundwater residence time in a high mountain aquifer system (Sacramento Mountains, USA): insights gained from use of multiple environmental tracers. *Hydrogeology Journal*, *24*(4), 787–804. https://doi.org/10.1007/s10040-016-1400-4

Lastennet, R., & Mudry, J. (1997). Role of karstification and rainfall in the behavior of a heterogeneous karst system. *Environmental Geology*, *32*(2), 114–123. https://doi.org/10.1007/s002540050200

Liu, Y., Wagener, T., & Hartmann, A. (2021). Assessing streamflow sensitivity to precipitation variability in karst-influenced catchments with unclosed water balances. *Water Resources Research*, *57*(1). https://doi.org/10.1029/2020WR028598

Long, A. J., & Valder, J. F. (2011). Multivariate analyses with end-member mixing to characterize groundwater flow: Wind Cave and associated aquifers. *Journal of Hydrology*, *409*(1–2), 315–327. https://doi.org/10.1016/j.jhydrol.2011.08.028

López-Moreno, J. I., Pomeroy, J. W., Morán-Tejeda, E., Revuelto, J., Navarro-Serrano, F. M., Vidaller, I., & Alonso-González, E. (2021). Changes in the frequency of global high mountain rain-on-snow events due to climate warming. *Environmental Research Letters*, *16*(9), 094021. https://doi.org/10.1088/1748-9326/ac0dde

Mann, H. B., & Whitney, D. R. (1947). On a test of whether one of two random variables is stochastically larger than the other. *The Annals of Mathematical Statistics*, *18*(1), 50–60. Retrieved from http://www.jstor.org/stable/2236101

McNutt, R. H. (2000). Strontium isotopes. In P. G. Cook & A. L. Herczeg (Eds.), *Environmental Tracers in Subsurface Hydrology* (pp. 233–260). New York: Spring Sceince+Business Media. https://doi.org/10.1007/978-1-4615-4557-6_8

Minvielle, S., Lastennet, R., Denis, A., & Peyraube, N. (2015). Characterization of karst systems using SIc-Pco2 method coupled with PCA and frequency distribution analysis. Application to karst systems in the Vaucluse county (Southeastern France). *Environmental Earth Sciences*, *74*(12), 7593–7604. https://doi.org/10.1007/s12665-015-4389-4

Mote, P. W., Hamlet, A. F., Clark, M. P., & Lettenmaier, D. P. (2005). Declining mountain snowpack in western North America. *Bulletin of the American Meteorological Society*, *86*(1), 39–50. https://doi.org/10.1175/BAMS-86-1-39

Musgrove, M., Solder, J. E., Opsahl, S. P., & Wilson, J. T. (2019). Timescales of water-quality change in a karst aquifer, south-central Texas. *Journal of Hydrology X*, *4*, 100041. https://doi.org/10.1016/j.hydroa.2019.100041

Neilson, B. T., Tennant, H., Stout, T. L., Miller, M. P., Gabor, R. S., Jameel, Y., et al. (2018). Stream centric methods for determining groundwater contributions in karst mountain watersheds. *Water Resources Research*, *54*(9), 6708–6724. https://doi.org/10.1029/2018WR022664

Neilson, B. T., Tennant, H., Strong, P. A., & Horsburgh, J. S. (2021). Detailed streamflow data for understanding hydrologic responses in the Logan River Observatory. *Hydrological Processes*, *35*(8), e14268. https://doi.org/10.1002/HYP.14268

Nerantzaki, S. D., & Nikolaidis, N. P. (2020). The response of three Mediterranean karst springs to drought and the impact of climate change. *Journal of Hydrology*, *591*, 125296. https://doi.org/10.1016/j.jhydrol.2020.125296

Olarinoye, T., Gleeson, T., Marx, V., Seeger, S., Adinehvand, R., Allocca, V., et al. (2020). Global karst springs hydrograph dataset for research and management of the world's fastest-flowing groundwater. *Scientific Data*, *7*(1), 59. https://doi.org/10.1038/s41597-019-0346-5

Ozyurt, N. N. (2008). Residence time distribution in the Kirkgoz karst springs (Antalya-Turkey) as a tool for contamination vulnerability assessment. *Environmental Geology*, *53*(7), 1571–1583. https://doi.org/10.1007/s00254-007-0811-x

Paces, J. B., & Wurster, F. C. (2014). Natural uranium and strontium isotope tracers of water sources and surface water–groundwater interactions in arid wetlands – Pahranagat Valley, Nevada, USA. *Journal of Hydrology*, *517*, 213–225. https://doi.org/10.1016/J.JHYDROL.2014.05.011

Parkhurst, D. L., & Appelo, C. A. J. (2013). *Description of input and examples for PHREEQC version 3: a computer program for speciation, batch-reaction, one-dimensional transport, and inverse geochemical calculations*. Reston, VA: U.S. Geological Survey. https://doi.org/10.3133/tm6A43

Payn, R. A., Gooseff, M. N., McGlynn, B. L., Bencala, K. E., & Wondzell, S. M. (2009). Channel water balance and exchange with subsurface flow along a mountain headwater stream in Montana, United States. *Water Resources Research*, *45*(11), 11427. https://doi.org/10.1029/2008WR007644

Pedregosa, F., Varoquaux, G., Gramfort, A., Michel, V., Thirion, B., Grisel, O., et al. (2011). Scikit-learn: Machine learning in Python. *Journal of Machine Learning Research*, *12*, 2825–2830. Retrieved from https://jmlr.csail.mit.edu/papers/v12/pedregosa11a.html

Perne, M., Covington, M. D., & Gabrovšek, F. (2014). Evolution of karst conduit networks in transition from pressurised flow to free surface flow. *Hydrology and Earth System Sciences Discussions*, *11*(6), 6519–6559. https://doi.org/10.5194/hessd-11-6519-2014

Pulido-Bosch, A., Padilla, A., Dimitrov, D., & Machkova, M. (1995). The discharge variability of some karst springs in Bulgaria studied by time series analysis. *Hydrological Sciences Journal*, *40*(4), 517–532. https://doi.org/10.1080/02626669509491436

Shuster, E. T., & White, W. B. (1971). Seasonal fluctuations in the chemistry of limestone springs: A possible means for characterizing carbonate aquifers. *Journal of Hydrology*, *14*(2), 93–128. https://doi.org/10.1016/0022-1694(71)90001-1

Smart, C. (2003, December 11). Alpine karst. In J. Gunn (Ed.), *Encyclopedia of Caves and Karst Science* (pp. 64–68). New York, NY: Taylor & Francis.

Spangler, L. E. (2001). Delineation of recharge areas for karst springs in Logan Canyon, Bear River Range, Northern Utah. In E. L. Kuniansky (Ed.), *U.S. Geological Survey Karst Interest Group Proceedings, St. Petersburg, Florida, Water-Resources Investigations Report 01-4011*. Reston, VA: U.S. Geological Survey. https://doi.org/10.3133/wri014011

Spellman, P., Breithaupt, C., Bremner, P., Gulley, J., Jenson, J., & Lander, M. (2022). Analyzing recharge dynamics and storage in a thick, karstic vadose zone. *Water Resources Research*, e2021WR031704. https://doi.org/10.1029/2021WR031704

Stevanović, Z. (2019). Karst waters in potable water supply: a global scale overview. *Environmental Earth Sciences*, *78*(23), 662. https://doi.org/10.1007/s12665-019-8670-9

Tennant, C. J., Crosby, B. T., & Godsey, S. E. (2015). Elevation-dependent responses of streamflow to climate warming. *Hydrological Processes*, *29*(6), 991–1001. https://doi.org/10.1002/hyp.10203

Tennant, H., Neilson, B. T., Miller, M. P., & Xu, T. (2021). Ungaged inflow and loss patterns in urban and agricultural sub-reaches of the Logan River Observatory. *Hydrological Processes*, *35*(4). https://doi.org/10.1002/hyp.14097

USGS. (2023). Cache Highline Canal near Logan, Utah - 10108400 and Logan River above state dam, near Logan, UT - 10109000. https://doi.org/10.5066/F7P55KJN

Veress, M. (2020). Karst types and their karstification. *Journal of Earth Science*, *31*(3), 621–634. https://doi.org/10.1007/s12583-020-1306-x

Wang, F., Chen, H., Lian, J., Fu, Z., & Nie, Y. (2020). Seasonal recharge of spring and stream waters in a karst catchment revealed by isotopic and hydrochemical analyses. *Journal of Hydrology*, *591*, 125595. https://doi.org/10.1016/j.jhydrol.2020.125595

Worthington. (1999). A comprehensive strategy for understanding flow in carbonate aquifers. In A. N. Palmer, M. V Palmer, & I. D. Sarawosky (Eds.), *Karst Modeling: Special Publication 5* (pp. 30–37). Charlottesville, VA: Karst Waters Institute.

Zoghbi, C., & Basha, H. (2019). Simplified physically based models for free-surface flow in karst systems. *Journal of Hydrology*, *578*, 124040. https://doi.org/10.1016/j.jhydrol.2019.124040

APPENDICES

Appendix A. Supplemental Figures

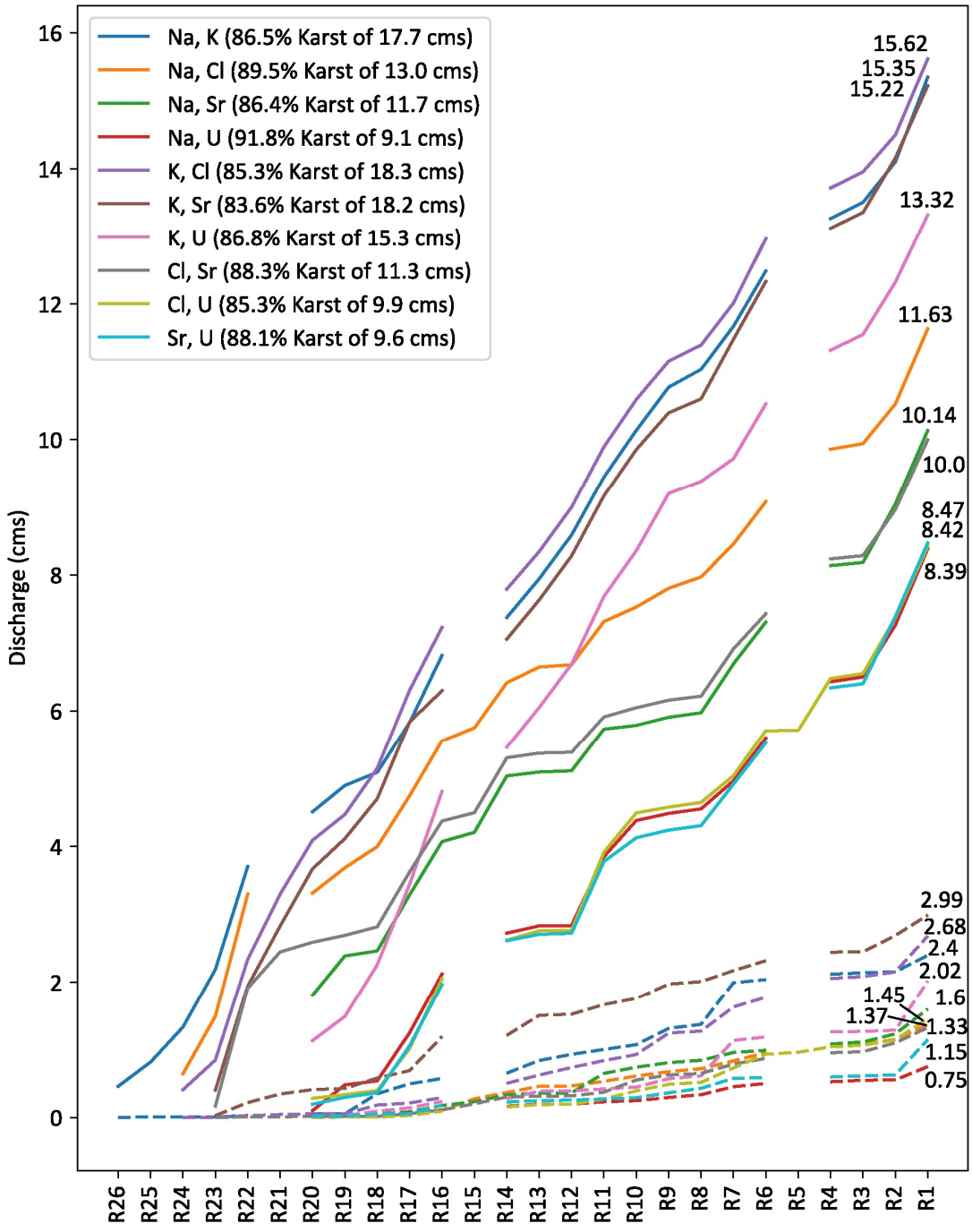

Fig. A 1. Cumulative median karst component discharge and the associated matrix component discharge for June two-solute balances. The dashed lines are the cumulative matrix component. The solid lines are the cumulative karst component.

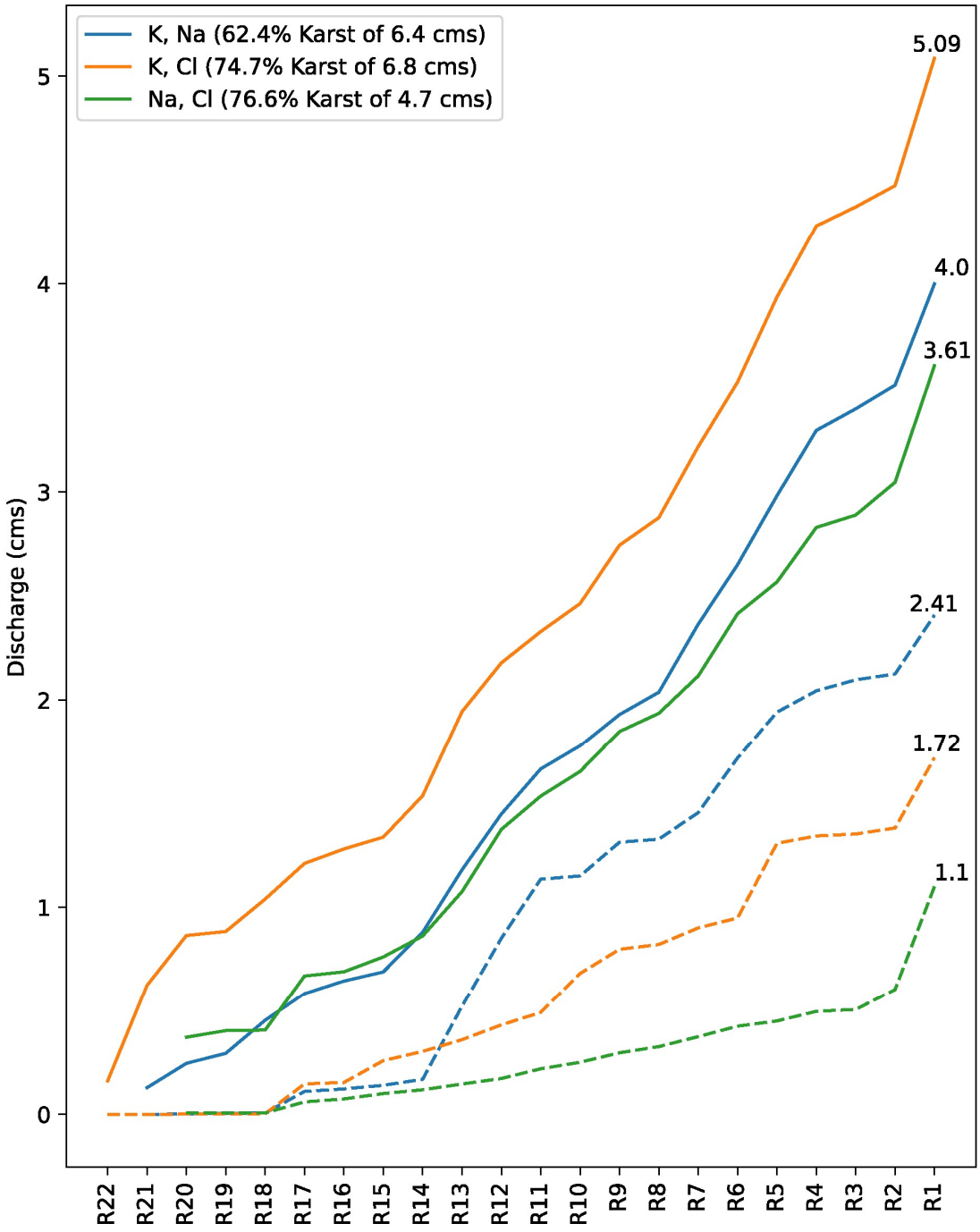

Fig. A 2. Cumulative median karst component discharge and the associated matrix component discharge for October two-solute balances. The dashed lines are the cumulative matrix component. The solid lines are the cumulative karst component.

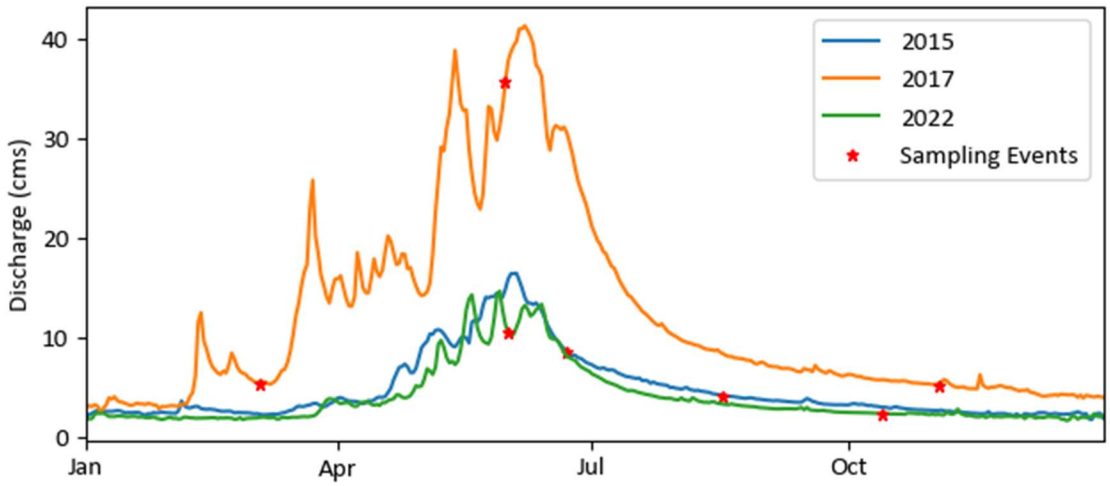

Fig. A 3. The hydrographs of Logan Canyon output (including Highline Canal Diversion) for 2015 (Neilson et al., 2018), 2017 (Lachmar et al., 2021), and 2022.

Appendix B. Supplemental Tables

Table B 1. Reference of site codes to local names.

Site	Site name
M0	Logan River at USGS gaging station at First Dam
D2.07	USGS stream gage at the Highline Canal Diversion
T6.1	Spring Hollow Creek Above Confluence with the Logan River
S7.35	Dewitt Springs above confluence with Logan River
M8.27	Logan River at Guinavah Campground Bridge
M9.19	Logan River at the Valhalla Summer Homes
M10.61	Logan River at Summer Home Site
M11.57	Logan River Below Card Canyon
M12.53	Logan River at ChokeCherry Campground
T14.79	Right Hand Fork above confluence with Logan River
M15	Logan River Above Right Hand Fork
S16.29	Tab Hollow Karst Spring
S16.31	China Row Spring Above Confluence with the Logan River
S16.89	Wood Camp Spring Above Confluence with the Logan River
M16.92	Logan River Above Wood Camp
S19.56	Logan Cave Spring Above Confluence with the Logan River
T19.74	Cottonwood Creek Confluence with the Logan River
M19.85	Logan River Above Cottonwood Creek
S20.69	Pullout Spring
M20.71	Logan River Above Pullout Spring
S22.02	Above Temple Fork Spring
M24.74	Logan River at Top of Dugway
S25.13	Bear Hollow Dugway Spring
S25.14	Temple Couloir
S25.9	Blind Hollow Spring
T26.03	Temple Fork above confluence with Logan River
M26.23	Logan River Above Temple Fork
S27.18	Ricks Spring above confluence with Logan River
M27.31	Logan River Above Ricks Spring
M30.09	Logan River at the Cattle Guard
T31.94	West Hodges Creek
T32.09	Theurer Creek
S32.76	Little Bear Creek Ranger Station Spring
M32.77	Logan River near Tony Grove
T33.06	Little Bear Creek
T34.14	Tony Grove Creek Above Confluence with the Logan River
S34.99	Wasatch Island Spring
M35.51	Logan River at Red Banks Campground

S35.92	Red Banks Beaver Pond Spring
S36.5	Bloomington Spring
T36.59	White Pine Creek Above Confluence with the Logan River
M37.31	Logan River at Daines Bridge
S38.51	Brush Canyon Spring
S39.04	6605 Spring
T39.18	Beaver Creek above confluence with Logan River
S39.18	Beaver Creek Leaching Hillslope
S39.22	Franklin Parking Lot Spring
S39.33	6720 Spring
M39.78	Logan River at Franklin Culvert (Bridge)
S40.23	Curley Spring
S40.39	Moe Spring
S40.45	Larry Spring
S40.52	Franklin Basin Horse Camp Spring
M41.22	Logan River Above Franklin Basin Beaver Complex
S42.28	Beaver Spring Seep Above Confluence with the Logan River
M42.33	Logan River near Franklin Basin
S42.8	Woodsey Spring
S42.88	Nounan Spring
M42.96	Logan River Above Nounan Spring
T43.63	Peterson Hollow Creek
S43.74	Franklin Basin Karst Spring
M43.83	Logan River Above Franklin Basin Karst Spring
S44.48	Lodge Spring
T45.27	Steep Hollow Creek
S45.3	Steep Hollow Spring
M45.75	Logan River Above Steep Hollow Spring
M48.87	Logan River near State Line
M50.08	Logan River below White Canyon Confluence
M55	Logan River below Corral Hollow
M56.95	Logan River below Gibson Lake Confluence

Table B 2. All data utilized for analysis.

Site	Date (2022)	Na mg/L	Ca mg/L	K mg/L	Mg mg/L	Cl mg/L	SO4 mg/L	Q cms	Sr ug/L	U ug/L	Sr87/ Sr86	U234/ U238	Water temp. C	pH	Sp cond. uS/cm	DO mg/L	mg CaCO3 /L
M0	6/2	3.10	45.86	0.36	12.17	4.85	3.12	8.891	52.2	0.235	0.71007	3.32	9.93	8.60	313	8.85	165
D2.07	6/2							1.291									
T6.1	6/2	1.74	58.35	0.45	10.33	1.50	5.71	0.506	67.5	0.578	0.70926	2.72	6.86	8.56	346	9.61	188
S7.35	6/2	2.89	49.08	0.30	11.23	4.67	5.38	0.630	64.2	0.357	0.70936	2.66	6.90	7.74	355	7.86	171
M8.27	6/2	2.97	43.54	0.34	11.70	4.52		8.028	48.8	0.175	0.71021	3.58	8.18	8.63	305	9.53	165
M9.19	6/2	3.06	44.12	0.34	11.79	4.44	2.13	7.823	45.0	0.181	0.71022	3.61	7.73	8.62	304	9.31	165
M10.61	6/2	3.00	45.29	0.35	11.95	4.37	2.11	8.557	44.7	0.178	0.71023	3.62	7.43	8.60	303	9.26	161
M11.57	6/2	2.98	44.88	0.35	12.11	4.34	2.11	7.943	45.3	0.176	0.71023	3.63	7.13	8.47	304	9.22	165
M12.53	6/2	2.78	43.17	0.34	11.73	4.27	2.11	8.913	44.7	0.173	0.71023	3.62	6.98	8.54	302	9.13	165
T14.79	6/2	4.34	56.12	0.60	16.80	6.76	8.96	0.204	103.1	0.582	0.71046	5.39	11.43	8.69	377	8.17	213
M15	6/2	2.77	44.15	0.34	11.87	3.94	1.93	8.271	42.5	0.163	0.71021	3.45	6.58	8.47	298	9.05	163
S16.29	6/2	8.51	49.01	0.43	16.64	10.14	2.76	0.001	51.2	0.231	0.71019	3.29	6.74	7.99	390	7.79	205
S16.31	6/2	27.17	57.99	0.55	21.78	53.53	8.03	0.007	65.0	0.297	0.71045	3.45	7.25	6.83	552	7.15	213
S16.89	6/2	0.83	40.09	0.22	17.84	0.76	1.54	1.573	23.6	0.147	0.71012	2.20	6.22	8.12	310	9.65	177
M16.92	6/2	2.89	42.39	0.36	10.95	4.04	1.71	6.382	47.7	0.149	0.71022	3.63	10.70	8.66	278		152
S19.56	6/1	1.18	45.83	0.36	16.33	0.94	2.57	0.081	41.3	0.184	0.70997	2.99	6.69	8.29	332	9.82	182
S19.56	6/2	1.18	45.83	0.36	16.33	0.94	2.57	0.068	41.3	0.184	0.70997	2.99	6.69	8.29	332	9.82	182
T19.74	6/1	0.95	50.86	0.30	14.30	0.86	2.53	0.333	43.7	0.228	0.70946	2.11	10.27	8.55	330	9.16	186
T19.74	6/2	0.95	50.86	0.30	14.30	0.86	2.53	0.295	43.7	0.228	0.70946	2.11	10.27	8.55	330	9.16	186
M19.85	6/1	2.90	41.94	0.36	10.74	4.13	1.69	6.506	47.6	0.141	0.71026	3.74	10.27	8.72	280		152
M19.85	6/2	2.90	41.94	0.36	10.74	4.13	1.69	6.461	47.6	0.141	0.71026	3.74	10.27	8.72	280		152
S20.69	6/1	4.88	61.39	0.69	20.43	6.17	11.34	0.002	80.1	0.336	0.71042	2.95	6.87	7.89	440		230
M20.71	6/1	2.79	42.74	0.35	10.74	3.84	1.58	6.427	47.0	0.137	0.71025	3.73	9.06	8.72	279		154
S22.02	6/1	7.47	45.05	0.42	11.67	10.56	1.87	0.003	44.8	0.144	0.71022	3.31	8.23	8.40	313	8.85	159
M24.74	6/1	2.73	43.90	0.36	10.88	3.56	1.78	6.601	46.8	0.139	0.71025	3.74	8.29	8.62	280		154
S25.13	6/1	1.41	49.44	0.37	13.86	1.38	1.68	0.018	42.9	0.134	0.71002	4.20	6.31	7.44	312		182
S25.14	6/1	4.34	51.77	0.69	17.59	6.12	4.80	0.071	105.8	0.427	0.71057	7.47	11.02	7.52	369		196
S25.9	6/1	5.33	52.48	0.64	17.91	8.63	3.09	0.003	96.8	0.336	0.71031	7.33	10.39	8.01	4	8.97	207
M26.23	6/1	2.82	43.93	0.36	11.04	3.54	1.35	5.603	42.4	0.131	0.71021	3.49	7.47	8.58	275	9.93	154
M27.31	6/1	3.04	43.05	0.38	10.83	3.84	1.71	4.531	42.4	0.130	0.71027	3.25	7.33	8.50	264	9.68	146
M30.09	6/1	2.92	41.78	0.36	10.41	3.76	1.73	4.539	41.8	0.122	0.71027	3.27	6.69	8.34	266	11.07	148

Site	Date (2022)	Na mg/L	Ca mg/L	K mg/L	Mg mg/L	Cl mg/L	SO4 mg/L	Q cms	Sr ug/L	U ug/L	Sr87/ Sr86	U234/ U238	Water temp. C	pH	Sp cond. uS/cm	DO mg/L	mg CaCO3 /L
T31.94	6/1	6.33	89.38	1.07	14.99	6.79	7.36	0.006	150.1	0.454	0.71020	2.62	6.34	7.35	510	5.40	267
T32.09	6/1	4.58	52.55	0.48	7.46	4.66	2.41	0.002	95.7	0.187	0.70973	2.85	9.92	7.85	331	8.10	173
S32.76	6/1	2.35	38.22	0.50	22.20	1.99	6.19	0.002	80.4	0.809	0.71231	3.36	8.24	7.63	362	10.88	196
M32.77	6/1	2.67	42.06	0.35	10.12	3.41	1.43	4.074	43.0	0.113	0.71027	3.26	5.62	8.47	264	7.76	146
M32.77	6/4	2.67	42.06	0.35	10.12	3.41	1.43	4.831	43.0	0.113	0.71027	3.26	5.62	8.47	264	7.76	146
T33.06	6/4	2.20	46.13	0.85	19.78	1.27	2.81	0.046	71.6	0.356	0.71130	3.06	14.34	8.04	342	6.38	193
T34.14	6/4	2.77	60.57	0.88	15.45	1.64	1.37	0.004	82.1	0.356	0.70963	2.57	12.52	7.88	372	6.12	203
S34.99	6/4	3.58	42.93	0.51	20.41	3.12	6.64	0.010	72.0	1.401	0.71163	3.76	13.90	8.36	337	6.61	185
M35.51	6/4	2.42	41.69	0.41	11.12	2.79	1.68	5.187	41.0	0.129	0.71028	3.25	11.53	8.61	266	8.99	143
S35.92	6/4	5.27	94.01	0.58	4.05	3.75	6.04	0.002	175.7	0.336	0.70937	4.04	7.11	7.22	433	6.78	232
S36.5	6/4	3.50	64.03	0.53	18.26	2.75	6.61	0.006	108.5	0.372	0.71104	3.91	7.75	6.80	413	9.06	221
T36.59	6/4	0.86	41.75	0.33	20.27	0.69	1.52	0.490	26.7	0.133	0.71036	2.10	9.56	8.32	314	7.29	177
M37.31	6/4	2.54	41.40	0.40	10.13	2.79	1.69	4.079	38.0	0.131	0.71025	3.41	10.40	8.45	261	9.12	139
S38.51	6/4	15.84	61.86	0.56	22.14	33.48	6.21	0.033	91.7	0.586	0.71141	5.11	8.46	7.07	506	6.12	221
S39.04	6/4	1.21	51.05	0.40	20.76	0.95	2.05	0.198	36.9	0.153	0.71025	4.67	5.88	6.92	367	9.25	205
T39.18	6/4	8.10	52.99	0.52	15.90	11.53	2.16	0.561	48.8	0.185	0.71036	4.57	9.81	7.85	359	9.23	183
S39.18	6/4	1.82	48.62	0.56	12.43	1.30	2.20	0.020	52.3	0.211	0.71020	2.97	5.55	6.83	302	5.90	163
S39.22	6/4	1.36	41.46	0.38	12.36	0.77	1.83	0.012	37.5	0.199	0.71019	3.28	5.29	7.22	268	8.14	147
S39.33	6/4	1.09	46.69	0.35	20.71	0.82	1.76	0.021	32.2	0.149	0.71032	2.59	6.79	7.62	338	9.53	187
M39.78	6/3	1.11	39.46	0.35	7.58	0.72	1.51	2.800	37.1	0.101	0.71015	2.78	10.40	7.70	228	8.91	123
M39.78	6/4	1.11	39.46	0.35	7.58	0.72	1.51	2.800	37.1	0.101	0.71015	2.78	10.40	7.70	228	8.91	123
S40.23	6/3	2.42	70.29	0.38	18.28	1.65	4.61	0.003	75.4	0.206	0.71032	4.53	7.04	7.45	439	8.78	236
S40.39	6/3	2.41	73.84	0.42	19.14	1.64	4.23	0.003	76.3	0.201	0.71031	3.65	6.86	7.56	436	8.55	240
S40.45	6/3	2.01	64.53	0.40	18.44	1.42	2.72	0.012	64.5	0.176	0.71028	3.85	6.63	7.43	396	8.29	219
S40.52	6/3	1.21	50.25	0.38	20.50	0.96	2.11	0.015	36.8	0.141	0.71024	4.55	5.79	6.64	360	9.18	197
M41.22	6/3	0.94	35.86	0.31	6.20	0.71	1.48	2.929	35.8	0.096			9.58	7.62	225	8.97	125
M42.33	6/3	0.95	36.38	0.32	6.12	0.70	1.47	2.997	36.0	0.093	0.71016	2.65	8.78	8.23	224	9.08	123
S42.88	6/3	1.37	52.31	0.35	15.26	1.13	2.25	0.028	43.4	0.143	0.71019	4.84	5.77	7.47	363	9.66	201.36
M42.96	6/3	0.94	36.08	0.34	5.77	0.68	1.43	2.975	34.7	0.085	0.71015	2.52	8.22	7.65	219	9.32	124.84
T43.63	6/3							0.035					14.92	8.57	299	8.83	
S43.74	6/3	1.07	43.51	0.40	6.65	0.78	1.61	0.406	42.6	0.112	0.71006	3.59	5.38	6.82	261	9.30	142.97
M43.83	6/3	1.02	32.82	0.29	5.27	0.69	1.45	2.426	35.1	0.080	0.71017	2.26	7.13	7.59	212	9.56	118.80
S44.48	6/3	0.93	41.35	0.33	6.57	0.75	1.65	0.128	38.7	0.093	0.71011	2.45	4.69	7.54	253	9.91	140.95

Site	Date (2022)	Na mg/L	Ca mg/L	K mg/L	Mg mg/L	Cl mg/L	SO4 mg/L	Q cms	Sr ug/L	U ug/L	Sr87/ Sr86	U234/ U238	Water temp. C	pH	Sp cond. uS/cm	DO mg/L	mg CaCO3 /L
T45.27	6/3	0.77	17.10	0.37	8.87	0.60	1.01	0.020	13.7	0.044	0.71074	1.98	9.90	7.63	153	8.73	86.59
S45.3	6/3	0.93	41.73	0.30	5.76	0.74	1.69	0.107	40.9	0.093	0.71008	2.38	4.47	7.47	252	10.28	140.95
M45.75	6/3	0.83	17.50	0.29	4.10	0.57	0.97	0.804	21.9	0.056	0.71049	1.71	8.91	7.47	122	9.02	66.45
M48.87	6/3	0.91	10.15	0.34	2.82	0.48	0.76	0.697	15.5	0.032	0.71076		8.04	7.78	70	9.03	44.30
M50.08	6/3	0.90	4.16	0.38	0.69	0.42	0.76	0.366	14.1	0.025	0.71091	1.55	6.78	7.12	28	9.20	24.16
M55	6/3	0.99	3.84	0.44	0.64	0.46	0.79	0.325	13.8	0.024	0.71093	1.47	7.37	7.26	31	9.39	28.19
M56.95	6/3	0.85	5.69	0.29	0.70	0.42	0.77	0.119	13.9	0.022	0.71082	1.46	8.03	7.16	35	8.81	26.18
M0	10/13	3.61	48.23	0.47	18.43	4.33	8.79	1.744	37.7	0.259	0.71005	3.70	9.16	8.64	367	10.16	202
D2.07	10/13							0.677									
T6.1	10/13	2.03	50.57	0.47	14.95	1.46	14.88	0.106	21.4	0.281	0.70933	3.51	6.12	8.44	353	10.42	188
S7.35	10/13	3.18	45.17	0.40	17.20	3.25	11.35	0.094	25.1	0.326	0.70957	3.14	8.03	7.78	356	9.43	196
M8.27	10/13	3.37	46.26	0.44	16.96	4.05	5.85	1.784	44.1	0.240	0.71034	4.71	8.53	8.55	352	10.69	186
M9.19	10/13	3.27	45.75	0.45	17.01	4.04	4.39	1.719	17.5	0.087	0.71036	4.80	9.12	8.75	350	10.22	196
M10.61	10/13	3.30	46.39	0.45	17.10	4.05	5.13	2.042	36.0	0.193	0.71036	4.78	9.16	8.73	351	10.25	192
M11.57	10/13	3.27	45.92	0.45	16.98	4.04	4.87	1.852	29.6	0.155	0.71037	4.80	9.09	8.72	352	10.42	196
M12.53	10/13	3.13	44.50	0.43	16.55	3.95	4.98	2.014	32.5	0.169	0.71036	4.81	8.78	8.69	353	10.35	196
T14.79	10/13	4.16	54.93	0.75	17.70	4.57	8.27	0.182	62.0	0.290	0.71051	5.62	9.14	8.60	404	9.63	224
M15	10/13	2.79	42.45	0.37	15.79	3.61	4.82	1.651	50.0	0.199	0.71033	4.67	7.98	8.64	347	10.17	194
S16.29	10/13	5.42	52.76	0.40	18.43	6.72	5.50	0.000	17.6	0.065	0.71017	3.29	9.08	7.63	385	4.36	200
S16.31	10/13	10.27	48.64	0.39	18.80	13.76	6.23	0.004	57.5	0.237	0.71044	3.50	8.61	7.71	423	4.43	210
S16.89	10/13	1.03	39.16	0.24	19.46	0.93	4.82	0.474	21.1	0.148	0.71035	3.13	6.37	7.80	325	10.09	182
M16.92	10/13	3.22	48.68	0.46	16.03	4.06	5.05	1.100	54.2	0.195	0.71033	5.19	7.03	8.78	353	10.58	202
S19.56	10/13	1.77	52.29	0.46	20.06	1.54	6.53	0.018	20.6	0.086	0.70999	4.58	7.91	8.15	399	9.93	226
S20.69	10/14	4.91	59.35	0.61	25.73	6.70	9.61	0.003	30.2	0.118	0.71046	3.14	6.84	7.43	483	9.34	257
M20.71	10/14	2.93	47.30	0.46	15.36	3.76	5.08	1.151	37.2	0.127	0.71034	5.26	4.80	8.42	363	10.65	202
M24.74	10/14	2.94	50.05	0.47	16.15	3.50	5.18	1.144	24.3	0.078	0.71033	5.30	5.09	8.29	364	10.56	202
S25.13	10/14	2.83	47.51	0.42	16.66	1.39	5.39	0.184	31.4	0.113	0.70996	6.76	7.23	7.47	353	9.64	196
S25.14	10/14	4.09	49.51	0.63	16.54	5.49	6.78	0.057	46.8	0.180	0.71061	7.34	11.04	7.61	315	7.32	200
S25.9	10/14	4.76	51.27	0.63	17.35	7.33	5.21	0.003	34.7	0.113	0.71031	7.23	9.21	7.60	399	6.94	204
T26.03	10/14	2.67	47.90	0.46	13.62	2.74	5.76	0.241	23.1	0.060	0.71052	5.03	4.72	8.38	357	10.54	196
M26.23	10/14	3.07	50.41	0.46	16.76	3.87	4.63	0.761	31.2	0.111	0.71029	4.78	6.67	8.44	366	10.68	208
S27.18	10/14	3.94	48.81	0.44	15.38	3.39	4.36	0.014	38.9	0.134	0.71004	5.74	7.24	7.57	364	8.93	200
M27.31	10/14	3.34	50.90	0.47	16.89	3.69	5.04	0.560	32.7	0.109	0.71038	4.09	7.05	8.55	365	10.29	208

Site	Date (2022)	Na mg/L	Ca mg/L	K mg/L	Mg mg/L	Cl mg/L	SO4 mg/L	Q cms	Sr ug/L	U ug/L	Sr87/ Sr86	U234/ U238	Water temp. C	pH	Sp cond. uS/cm	DO mg/L	mg CaCO3 /L
M30.09	10/14	2.75	49.77	0.42	16.57	3.66	5.05	0.652	50.6	0.179	0.71039	4.13	8.36	8.56	363	10.06	204
T32.09	10/14	5.13	82.49	0.78	10.96	5.02	5.43	0.006	36.6	0.057	0.70962	2.91	8.35	7.67	450	6.40	248
S32.76	10/14	2.38	38.37	0.48	22.85	2.00	8.32	0.001	31.8	0.276	0.71231	3.37	8.31	7.91	359	10.56	196
M32.77	10/14	2.71	47.85	0.45	16.43	3.48	4.64	0.596	34.8	0.125	0.71039	4.21	11.21	8.66	345	8.97	196
T33.06	10/14	2.81	56.17	1.10	25.74	2.45	5.15	0.002	69.1	0.297	0.71159	3.31	9.77	8.10	446	8.00	250
T34.14	10/14	4.36	91.49	0.81	21.84	3.90	12.56	0.000	45.1	0.173	0.70964	2.71	8.24	7.42	556	5.12	300
S34.99	10/14	3.20	38.74	0.62	18.47	3.14	6.95	0.005	49.8	0.820	0.71168	3.76	9.99	8.43	332	8.93	185
M35.51	10/14	2.53	48.39	0.45	16.72	3.01	4.31	0.595	45.9	0.155	0.71036	4.30	10.80	8.60	351	9.12	201
S35.92	10/14	5.10	92.02	0.53	3.98	3.74	5.19	0.002	114.4	0.174	0.70937	4.05	7.50	7.33	443	7.57	241
S36.5	10/14	3.31	62.73	0.48	18.23	2.61	7.60	0.006	77.0	0.208	0.71112	4.03	7.99	7.54	416	8.96	225
M37.31	10/14	2.46	49.36	0.46	17.24	2.89	4.40	0.611	29.9	0.101	0.71035	4.42	10.18	8.48	356	9.05	229
S38.51	10/14	13.08	63.23	0.57	22.75	23.48	6.09	0.008	58.6	0.271	0.71139	5.09	8.38	7.53	484	4.07	214
S39.04	10/14	1.49	49.81	0.41	19.25	1.09	4.97	0.207	29.0	0.104	0.71023	5.35	6.57	7.56	372	8.46	210
T39.18	10/14	43.67	79.59	0.77	20.78	77.70	5.05	0.001	27.1	0.046	0.71047	3.84	10.69	7.64	704	6.25	258
S39.18	10/14	1.73	51.42	0.58	12.93	1.15	3.97	0.001	21.5	0.075	0.71022	2.97	8.49	7.53	340	5.94	185
S39.22	10/14	1.70	53.34	0.76	15.55	1.06	4.30	0.024	33.7	0.159	0.71019	3.30	8.78	7.65	334	6.30	187
S39.33	10/14	1.47	52.09	0.42	22.59	1.10	4.61	0.002	18.0	0.072	0.71027	2.94	6.60	8.29	398	9.27	225
M39.78	10/14	1.46	48.29	0.44	15.74	1.08	4.37	0.200	21.8	0.081	0.71019	4.23	8.37	8.41	332	9.41	185
M39.78	10/15	1.46	48.29	0.44	15.74	1.08	4.37	0.185	21.8	0.081	0.71019	4.23	8.37	8.41	332	9.41	185
S40.23	10/15	2.18	71.14	0.38	18.09	1.55	3.84	0.001	52.1	0.132	0.71032	3.64	7.06	7.45	440	8.00	246
M41.22	10/15	1.40	46.99	0.40	15.43	1.00	4.36	0.302	34.8	0.137	0.71016	4.42	5.06	8.50	328	10.26	186
S42.28	10/15	1.45	48.54	0.43	13.77	0.99	4.35	0.037	40.5	0.158	0.71010	4.80	6.32	7.50	333	7.34	190
M42.33	10/15	1.42	45.51	0.39	15.28	0.99	4.50	0.315	15.5	0.055	0.71017	4.40	5.87	8.50	327	10.16	192
S42.88	10/15	1.58	51.73	0.43	18.19	1.20	4.63	0.059	19.8	0.073	0.71023	5.37	5.99	7.50	372	8.59	207
M42.96	10/15	1.37	45.71	0.42	15.29	0.96	4.36	0.240	19.9	0.072	0.71016	4.23	6.74	8.57	318	9.86	182
S43.74	10/15	1.56	48.43	0.48	15.06	1.01	4.50	0.114	44.2	0.172	0.71010	5.39	5.69	7.59	328	8.82	184
M43.83	10/15	1.30	45.11	0.41	15.77	0.94	4.80	0.156	20.2	0.069	0.71020	3.29	7.93	8.58	318	9.85	182
S44.48	10/15	1.28	44.28	0.41	15.61	0.93	4.10	0.297	30.5	0.107	0.71019	3.33	5.47	7.50	327	8.85	180
T45.27	10/15	1.11	36.56	0.44	21.50	0.70	3.22	0.005	11.7	0.069	0.71056	2.17	7.32	8.52	310	9.12	177
M45.75	10/15	0.96	42.82	0.35	25.65	0.96	4.82	0.011	21.1	0.121	0.71049	2.03	8.25	8.62	362	9.36	215

Note. The data collected during the synoptic sampling event in June is placed above the data collected during the synoptic sampling event in October. The data collected for each synoptic sampling event is then sorted by river distance.